Gondwana Research 154 (2026) 236–257

Contents lists available at ScienceDirect

Gondwana Research

journal homepage: www.elsevier.com/locate/gr

Research Paper

Water circulation, redox, and productivity dynamics shaped late Ediacaran ecosystems: Insights from trace elements and combined Sr–Cr–Cd isotopes in the Corumbá Group, Brazil

Henrique Albuquerque Fernandes [a,*], Paulo César Boggiani [a], Jesper Allan Frederiksen [b], Thales Pescarini [c], Vinicius Cardoso Lucas [d], Gustavo Paula Santos [e], Eric Elias [e], Marly Babinski [a], Juliana Leme [a], Catherine V. Rose [f], Ricardo Ivan Ferreira Trindade [g], Robert Frei [b]

[a] Instituto de Geociências, Universidade de São Paulo, Rua do Lago, 562 São Paulo, Brazil
[b] Department of Geosciences and Natural Resources Management, University of Copenhagen. Øster Voldgade, 10, Copenhagen, Denmark
[c] Department of Earth and Planetary Sciences, Yale University. 210 Whitney Avenue, New Haven, USA
[d] Instituto de Geociências, Universidade Estadual de Campinas, Rua Carlos Gomes 250, 13083-855 Campinas, Brazil
[e] Faculty of Geosciences and MARUM, Center for Marine Environmental Sciences, University of Bremen, Leobener Strasse 8, 28359 Bremen, Germany
[f] School of Earth and Environmental Sciences, University of St Andrews, Fife KY16 9TS, UK
[g] Instituto de Astronomia, Geofísica e Ciências Atmosféricas, Universidade de São Paulo, Rua do Matão, 1226 São Paulo, Brazil

ARTICLE INFO

Keywords:
Cr isotopes
Cd isotopes
Corumbá Group
Ediacaran
Redox conditions

ABSTRACT

The relationship between marine oxygenation and early animal evolution remains a highly debated topic. Recent research suggests that, rather than absolute atmospheric O_2 threshold levels, the main factor controlling early animal distribution was long-term local marine redox conditions. To explore this hypothesis, we present trace element data along with Sr, Cr, and Cd isotopes in carbonate rocks from the late Ediacaran Corumbá Group, Brazil, obtained from drill cores of the GRIND-ECT project. This multiproxy approach is designed to constrain basin water circulation, redox conditions, and bioproductivity levels from ca. 565 to 540 Ma, ultimately aiming to reconstruct the paleoceanographic scenario in which early animal colonization occurred in the Corumbá Basin. Redox-sensitive metal abundances indicate a contrasting redox scenario, with predominant anoxia in the Bocaina Formation and expanded oxia in the overlying Tamengo Formation. This interpretation is further reinforced by Cr isotopes, whereby $\delta^{53}Cr$ passes from low values in the range of Bulk Silicate Earth to positively fractionated values upsection. Two negative $\delta^{53}Cr$ excursions in the Tamengo Formation are interpreted as anoxic intervals. $^{87}Sr/^{86}Sr$ values decrease from 0.7100 in the Bocaina Formation to late Ediacaran values around 0.7085 in the Tamengo Formation. These radiogenic values in the Bocaina Formation are attributed to post-depositional diagenesis of Sr-depleted dolostones. Lastly, variable $\delta^{114}Cd$ in the Bocaina Formation indicate contrasting productivity levels during highstand and flooding periods. The two anoxic intervals in the Tamengo Formation exhibit anomalous negative $\delta^{114}Cd$ values, which may be linked to widespread eutrophication. Our study, combined with compilations of redox and fossil data, reveals that the Corumbá Basin evolved from a predominantly anoxic setting dominated by microfossils in the Bocaina Formation, to a connected marine setting in the Tamengo Formation. This later phase featured a deeper redoxcline and was dominated by fossils of bio-mineralizing animals, representing a near-optimal environment for early animal benthic colonization.

1. Introduction

The potential relationship between oxygen levels and early metazoan evolution has long been studied and discussed in the literature (Nursall, 1959; Berkner and Marshall, 1965; Knoll, 1992; Knoll and Sperling, 2014; Mills and Canfield, 2014). Estimates point that an atmospheric oxygen threshold of 0.5–4% PAL (present atmospheric levels), necessary to sustain animal metabolism (Mills et al., 2014; Cole et al., 2020), may

* Corresponding author.
E-mail address: henriqueaf@usp.br (H.A. Fernandes).

https://doi.org/10.1016/j.gr.2026.01.006
Received 29 September 2025; Received in revised form 9 January 2026; Accepted 10 January 2026
Available online 4 February 2026

have been reached as early as 1400 Ma (Zhang et al., 2016; 2021), approximately 600 myr before the presumed origin of metazoans based on molecular clock estimations (dos Reis et al., 2015; Dohrmann and Wörheide, 2017). However, rather than absolute atmospheric oxygen concentrations, recent studies in Ediacaran successions suggest that the local long-term marine redox state was the major factor limiting early animal distribution (Cui et al., 2016; Bowyer et al., 2017; Evans et al., 2018, 2022; Wood and Erwin, 2017).

In modern oceans, the seawater redox state is primarily controlled by local hydrodynamics, productivity levels, and temperature (mainly dictated by latitude) (Algeo and Lyons, 2006; Bowyer et al., 2017). The shape of marine basins, coastal bathymetry, wind regime, and sea-level dictate local surface seawater circulation (Thiede and Jünger, 1992). Regions with more intense ocean circulation tend to present increased dissolved O_2, while restricted, stagnant water bodies or areas with sluggish circulation are prone to developing Oxygen Minimum Zones (OMZs) at depth through redox-stratification (Brandt et al., 2010; Thamdrup et al., 2012), occasionally reaching sulfidic conditions (Scholz, 2018). In this case, surface oxygenated waters are separated by anoxic/sulfidic deep waters by a redoxcline. Primary productivity, in turn, is chiefly limited by nutrient availability and light intensity (Rühlemann et al., 1999). Upwelling zones, for instance, where primary productivity is high due to the influx of nutrient-rich bottom waters, often experience surface water oxygen depletion through organic matter oxidation (Fuenzalida et al., 2009), while downwelling currents regularly inhibit deep nutrients from reaching surface waters (Hanson et al., 2005) and carry O_2-rich waters towards mid-depths (Yamamoto et al., 2015). Latitude also dictates the amount of dissolved oxygen in surface waters, given that O_2 is more soluble in the seawater at lower temperatures (Richards, 1958), ultimately resulting in a latitudinal gradient in oceanic dissolved O_2.

A similar circulation-productivity-redox interplay appears to have operated in the Ediacaran seas (Bowyer et al., 2017). Over most of the Ediacaran, oceans presented intense water column redox-stratification, with an upper layer of well-mixed oxygenated surface waters overlying ferruginous (anoxic and Fe-rich) bottom waters and sulfidic wedges on continental shelves (Canfield et al., 2008; Li et al., 2010; Frei et al., 2013). Such conditions, however, were highly dynamic and subject to spatial and temporal heterogeneity. A growing body of evidence based on detailed chemostratigraphic studies shows that basins that experienced variable connectivity to open ocean waters, such as the Yangtze Platform (South China), were prone to prolonged anoxia, with brief oxic periods during highstand intervals and consequent basin connection (Ostrander et al., 2019, 2020; Xu et al., 2022; Ostrander, 2023), while basins with a permanent connection with the open ocean developed continued oxia, such as the basin in which the Nama Group (Namibia) sediments were deposited (Wood et al., 2015; Tostevin et al., 2016b). In these basins, intense colonization of benthic environments by early animals occurred precisely during periods of oxygenation (Bowyer et al., 2017). Therefore, constraining local circulation and productivity is vital to correctly assess the relationship between redox conditions and metazoan distribution in each basin, and establish whether they can be correlated globally.

The Corumbá Group (Brazil) represents a late Ediacaran basin situated in Western Gondwana and includes carbonate successions with a rich fossiliferous content (Fairchild et al., 2012). Although it serves as an exceptional archive for paleoenvironmental research, key paleoceanographic characteristics of the Corumbá Basin—such as its redox history and levels of primary productivity—remain poorly constrained. To explore these open questions, we have analyzed carbonate rocks from the Corumbá Group for trace elements and strontium, chromium, and cadmium isotopes. This multiproxy approach, combined with extensive available paleontological data, offers new insights into the evolution of the Corumbá Basin, its associated biota, and for comprehending Ediacaran ecosystems.

2. Chromium isotope systematics

Chromium (Cr) is a redox-sensitive element (RSE), that usually occurs either as trivalent Cr(III) or hexavalent Cr(VI) in natural systems. Cr isotopes fractionate during oxi-reduction reactions, given that Cr(VI) bounds are more stable than those of Cr(III), thus always enriching the Cr(VI)-pool in the heavier isotope (^{53}Cr) with respect to the lighter isotope (^{52}Cr) (Schauble et al., 2004).

Oxidation of Cr(III) in soils by oxidative weathering releases the more mobile Cr(VI) into catchments and rivers, ultimately causing the riverine input into the ocean to be ^{53}Cr-enriched (Ellis et al., 2002; Oze et al., 2007; Berger and Frei, 2014; Frei et al., 2014; Miletto et al., 2021). Subsequently, the Cr isotope composition of the ocean is chiefly controlled by local redox conditions and primary productivity (Bonnand et al., 2013; D'Arcy et al., 2017; Janssen et al., 2020), either preserving the land-derived positive signature or causing isotopic offsets, mostly after Cr(VI) reduction. Cr is removed from the ocean mainly after reduction to the particle-reactive Cr(III) species, being scavenged onto settling particles in reducing and anoxic sediments (Reinhard et al., 2014; Wang et al., 2023). These removals account for more than 90 % of the total Cr sink influx, while the rest corresponds to oxic sediments sink (Reinhard et al., 2013).

The δ^{53}Cr of modern seawater ranges from +0.13 to +1.53 ‰ (Bonnand et al., 2013; Scheiderich et al., 2015; Paulukat et al., 2016), similar to modern rivers, whose δ^{53}Cr spans from +0.08 to +1.33 ‰ (Frei et al., 2014; Paulukat et al., 2015; D'Arcy et al., 2017). In the ocean, Cr(VI) can undergo reduction to Cr(III) through biotic (Pereira et al., 2015; Farkaš et al., 2018) and abiotic (Kitchen et al., 2012; Frank et al., 2019; Wang et al., 2023) pathways. These processes have distinct Cr isotope fractionation factors (ε). For instance, Cr(VI) reduction by Fe-bearing clays has ε spanning from −4.9 to −1.3 ‰ (Joe-Wong et al., 2021), while ε relative to Cr reduction by bacteria ranges from −0.4 to −5.0 ‰ (Sikora et al., 2008; Basu et al., 2014; Chen et al., 2019a; b; Zhang et al., 2019).

Cr stable isotopes in carbonate rocks have been widely used as a proxy to track atmospheric and seawater oxygenation in the geological record (e.g., Frei et al., 2009; 2011; Rodler et al., 2015; 2016; Gilleaudeau et al., 2016; Caxito et al., 2018; 2023; Klaebe et al., 2021; Frederiksen et al., 2022a; b; Rugen et al., 2022; Fernandes et al., 2025a). This application assumes that carbonate minerals reliably preserve the Cr isotope composition of the water in which they are formed. Laboratory experiments show that Cr fractionation during incorporation into calcite is negligible considering natural seawater conditions (Rodler et al., 2015), thus rendering carbonate $\delta^{53}Cr_{auth}$ to faithfully represent the seawater Cr isotope signal.

3. Cadmium isotope systematics

In the modern seawater, cadmium (Cd) presents a nutrient-like behavior, showing depletion in the photic zone due to phytoplankton uptake and progressive enrichment in deeper waters prompted by organic matter remineralization (Boyle et al., 1976; Lacan et al., 2006; Ripperger et al., 2007; Abouchami et al., 2014). This biologically-driven vertical profile in the water column is similar to the distribution of phosphate, which is the ultimate limiting nutrient in the ocean. The exact biological role of Cd in organisms remains uncertain. It may be used in the cadmium carbonic anhydrase enzyme (Cd-CA), a variant of the Zn-CA enzyme (Price and Morel, 1990). However, it is also possible that Cd serves no specific biological function and is instead inadvertently incorporated by organisms due to its chemical similarity to Zn (Hohl et al., 2017). The Cd isotope composition of seawater varies inversely with its concentration, as phytoplankton preferentially uptakes the lighter ^{110}Cd isotope with respect to the heavier ^{114}Cd isotope (Ripperger et al., 2007; Abouchami et al., 2011). This selective uptake results in surface waters with higher δ^{114}Cd and deep waters with lower and homogeneous δ^{114}Cd after organic matter remineralization,

concomitant Cd release, and water mass mixing at greater depths (Ripperger et al., 2007; George et al., 2019; Sieber et al., 2019).

Cd enters the ocean mainly via rivers and aeolian dust, with minor participation of hydrothermal fluxes (George et al., 2019; Bryan et al., 2021). The riverine and aeolian inputs have a similar Cd isotope composition around + 0.1 ‰ (Lambelet et al., 2013; Bridgestock et al., 2017), while the hydrothermal influx present a wide range of δ^{114}Cd, from −0.45 to +0.39 ‰ (Schmitt et al., 2009). The main sink of Cd from the ocean is organic matter bound Cd in continental margin sediments, with a relatively heavy Cd isotope composition from 0.08 to 0.39 ‰ (Janssen et al., 2019). In the case of suboxic to anoxic margin sediments, sulfide precipitation can also be a significant (and potentially dominant) Cd sink in the form of CdS, with lighter isotope composition down to −0.07 ‰ (Guinoiseau et al., 2019; Bryan et al., 2021). The adsorption of Cd onto Fe-Mn particulate is also a pathway of Cd removal from the ocean, although to a minor extent and impinging no significant isotopic fractionation (Bryan et al., 2021).

Considering that the magnitude of seawater δ^{114}Cd in shallow settings varies as a function of primary productivity and that carbonate minerals faithfully record the seawater Cd isotope composition, Cd isotopes from carbonate rocks can be a reliable archive for past marine primary productivity (Hohl et al., 2017; Druce et al., 2022; Frederiksen et al., 2022a; b).

4. Geological setting

4.1. Geology of the southern Paraguay belt and Corumbá group

The Paraguay Belt is a Neoproterozoic fold-thrust belt formed in the southeastern margin of the Amazonia Craton, specifically at the eastern border of the Rio Apa Terrane, when it collided with the Paranapanema and São Francisco cratons during the Brasiliano Orogenic Cycle, from the Ediacaran to early Cambrian (Alvarenga and Trompette, 1993; Trompette et al., 1998). The belt is divided into the northern and southern branches, whose geological evolution was similar during the late Cryogenian to early Ediacaran and distinct during the mid Ediacaran to early Cambrian, as recorded in sedimentary successions (Alvarenga et al., 2009; Babinski et al., 2018; Fernandes et al., 2025a). In the southern sector of the Paraguay Belt, the predominantly Ediacaran Corumbá Group represents the last sedimentation phase, possibly in a foreland setting (Campanha et al., 2011; McGee et al., 2018; Leite et al., 2024), although the precise timing of basin inversion is still unclear.

The Corumbá Group is divided into six units, Cadiueus, Cerradinho,

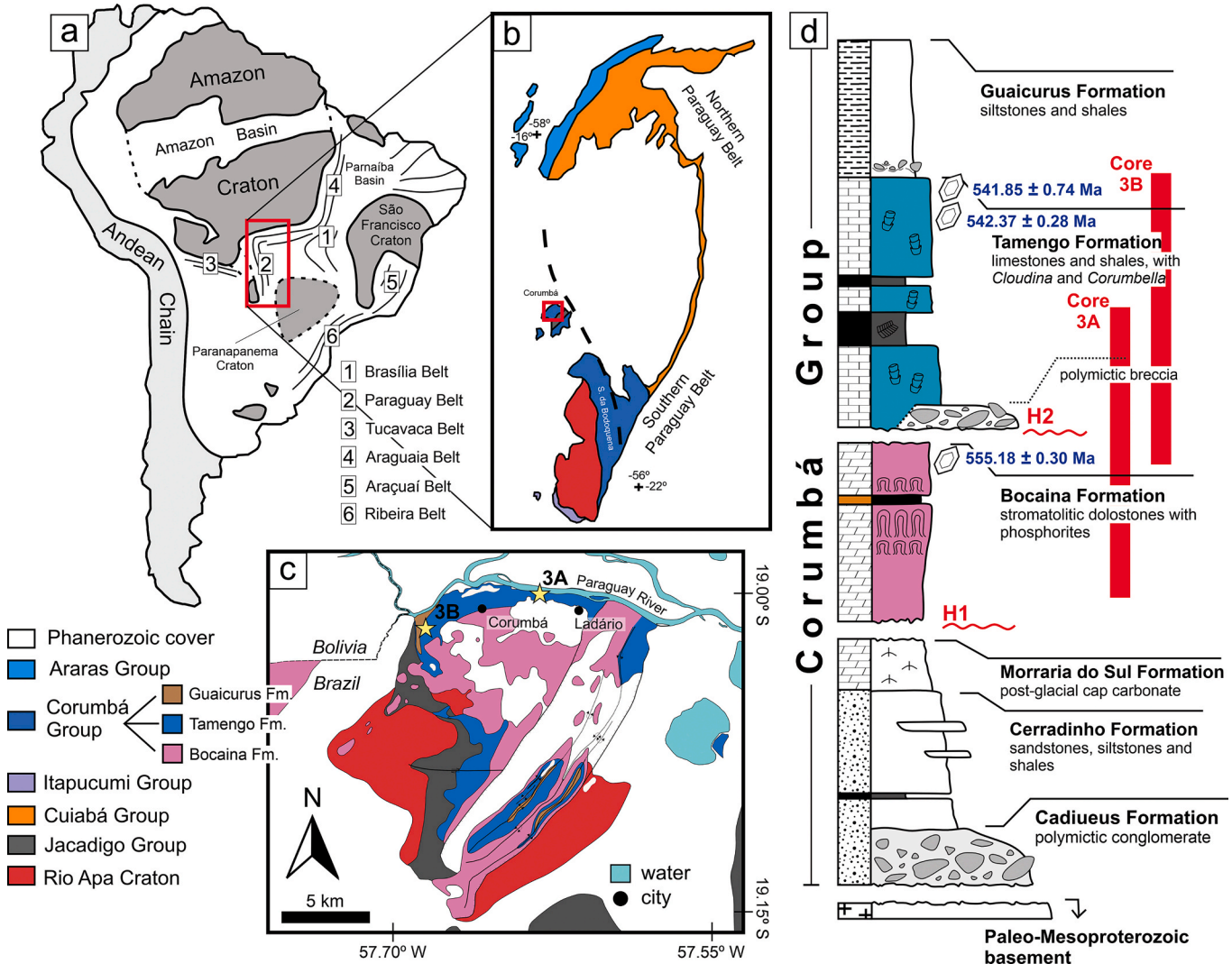

Fig. 1. (a) Schematic tectonic map of South America with main cratonic terranes and Neoproterozoic mobile belts. (b) Tectonic map of the Paraguay Belt and adjacent areas (after Parry et al., 2017). Red rectangle denotes the area in (c). (c) Geologic map of the Corumbá area with indication of the drill sites 3A and 3B. (d) Schematic stratigraphic column of the Corumbá Group, with indication of the stratigraphic position of cores 3A and 3B (after Fernandes et al., 2025b). U-Pb ash bed zircon ages are from Parry et al. (2017).

Morraria do Sul, Bocaina, Tamengo, and Guaicurus formations, from base to top (Fig. 1) (Almeida, 1965; Boggiani, 1998; Fernandes et al., 2025a). The Cadiueus and Cerradinho formations are the Cryogenian basal siliciclastic units of the Corumbá Group, comprising polymictic conglomerates and arkosic sandstones, respectively (Boggiani, 1998). They represent glacial outwash fans (Gaucher et al., 2003), possibly related to the Marinoan Glaciation (Hiatt et al., 2020). The Morraria do Sul Formation constitutes the early Ediacaran post-glacial cap carbonate phase formed during a major transgression over the Rio Apa Terrane (Fernandes et al., 2025a). The Bocaina Formation overlies the Cerradinho and Morraria do Sul formations over an erosive surface that represents a major hiatus in sedimentation (H1 in Fig. 1). Stromatolitic dolomites, breccias, phosphorites, and shales of the Bocaina Formation represent a reef-rimmed carbonate shelf (Boggiani et al., 1993; Hippertt et al., 2023), hosting a diverse microfossil content (Morais et al., 2021; 2024), although macrofossils are absent. The Bocaina-Tamengo limit is characterized by an erosive surface (H2 in Fig. 1), above which occur thick layers of polymictic breccia in slope and foreslope sections, deposited during a major regression in lowstand wedges (Fernandes et al., 2022; Fernandes et al., 2025b), and a hiatus in proximal shelf sections. The Tamengo Formation upwards presents limestones and shales, with metazoan fossils, namely *Cloudina* sp. (e.g., Walde et al., 2015; Adorno et al., 2017; Afonso et al., 2024), *Corumbella werneri* (e.g., Pacheco et al., 2018; Osés et al., 2022), and *Paraconularia ediacara* (Leme et al., 2022), as well as macroalgae (Diniz et al., 2021), vendotaenia (Gaucher et al., 2003; Becker-Kerber et al., 2022), and ichnofossils (Parry et al., 2017). The Tamengo Formation represents a storm-dominated carbonate ramp developed during a major transgression after ca. 550 Ma, considering correlations based on carbon isotope chemostratigraphy and fossil content (de Oliveira et al., 2019; Amorim et al., 2020; Ramos et al., 2022; Fernandes et al., 2024). Lastly, the Guaicurus Formation encompasses siltstones and shales formed during the last transgressive phase of the Corumbá Basin (Walde et al., 2015; Fazio et al., 2019).

The age of the uppermost Bocaina Formation is known through a volcanic ash layer that yielded a U-Pb zircon age of 555.18 ± 0.30 Ma (Parry et al., 2017). Additionally, a U-Pb dolomite age of 571 ± 9 Ma was obtained for the lower Bocaina Formation at the Serra da Bodoquena region (Morais et al., 2024) (Fig. 1). Within this uncertainty range, the base of drill core 3A (see next section) is thought to be around 565 Ma, based on carbon isotope correlations (Fernandes et al., 2025b). Two ash beds at the upper Tamengo Formation yielded U-Pb zircon ages of 542.37 ± 0.28 Ma and 541.85 ± 0.75 Ma, indicating a terminal Ediacaran sedimentation age (Parry et al., 2017), which agrees with the presence of fossils attributable to the Nama Assemblage (550–538 Ma) in this unit.

4.2. GRIND-ECT cores 3A and 3B

The samples analyzed in this study were obtained from drill cores 3A and 3B (Fig. 2) of the GRIND-ECT project (Geological Research through Integrated Neoproterozoic Drilling – Ediacaran-Cambrian Transition) of ICDP (International Continental Scientific Drilling Program) (Rose et al., 2019). Core 3A (−19.00°, −57.62°) was drilled at Porto Sobramil, in Corumbá (Fig. 1), and presents limestones and shales from the Tamengo Formation down to 55.24 m depth, where it sharply transitions to dolomites of the Bocaina Formation, extending to the base of the core at 182.95 m (Fig. 2). Core 3B (−19.02°, −57.68°) was drilled at the Corcal Mine, also located in the Corumbá area (Fig. 1). It contains limestones and shales from the Tamengo Formation in the top 114.58 m, followed by 8.45 m of dolomites from the Bocaina Formation at the bottom. For detailed sedimentological and stratigraphic data from cores 3A and 3B, the reader is referred to Fernandes et al. (2025b).

In both cores, the Bocaina Formation presents essentially dolograinstones, dolomite breccias, and microbialites, mainly stromatolites and oncolites in a transgressive systems tract followed by a highstand systems tract at the top. In core 3A, a maximum flooding surface separates these two systems tracts at ca. 100 m depth. The Tamengo Formation displays grainstones, mudstones, and black shales, also arranged in a transgressive and highstand systems tracts succession, with a maximum flooding surface at ca. 60 m depth in core 3B. Both sections are attributed to relatively shallow marine environment in the Corumbá Basin, with the Bocaina Formation representing a carbonate-dominated tidal flat and the Tamengo Formation denoting a slightly deeper carbonate ramp with deposition of black shales during low-energy periods (Boggiani et al., 1993; Amorim et al., 2020; Hippertt et al., 2023). The abrupt contact between the Tamengo and Bocaina formations characterizes a sequence boundary, with an erosional gap of ca. 5 My, from ca. 555 to 550 Ma, as suggested by the integration of radiometric ages, fossil content, and carbon isotope correlations (Fernandes et al., 2025b).

5. Methods

5.1. Sampling and sample preparation

Samples from cores 3A and 3B were collected avoiding zones with visible post-depositional alteration, brecciation, veins, and irregular bedding. Only carbonate samples were collected, as this study focuses on carbonate geochemistry. Samples were slabbed and polished with sandpaper to remove metal contaminations from the saw. Lastly, slabs were powdered down to 200 mesh using an agate mixer mill. A total of 37 samples were analyzed for trace elements and Sr isotopes, and, among these, 28 were analyzed for Cr isotopes and 19 for Cd isotopes. Supplementary Data (Table S1) presents the depth and geological formation of each sample.

5.2. Major and trace elements

All analytical procedures follow the methods described by Fernandes et al. (2025a). Around 600 mg of powdered samples were dissolved in 4 mL 0.5 N HNO_3 and subsequently diluted to 50 mL with ultra-pure water (Milli-Q; 18 MΩ resistivity). The solutions were analyzed for 48 elements with an Inductively Coupled Plasma Mass Spectrometer (ICP-MS) quadrupole instrument iCAP-Q from Thermo Scientific at the University of Copenhagen. The standard material NIST 1643f and a diluted Reagecon ICP-Multielement Standard with 23 elements were used for calibration. Furthermore, the J-Do1 dolomite standard material (Imai et al., 1996) was also analyzed to evaluate the accuracy of the geochemical data. The results for the J-Do1 standard were reported by Fernandes et al. (2025a).

In cross-plots, we considered $p < \alpha = 0.01$ to be statistically significant. Rare earth elements distribution diagrams were made after normalization as per Post-Archean average Australian Shale (PAAS; McLennan, 1989). Dy/Sm ratios were calculated to represent the magnitude of middle rare earth elements (MREE) enrichments over light rare earth elements (LREE). Cerium anomalies were calculated using the geometric equations of Lawrence et al. (2006):

$$(Ce/Ce^*)_n = (Ce)_n \times (Nd)_n \Big/ (Pr)_n^2 \quad (1)$$

and trace metals (TM) enrichment factors (EF) were calculated as:

$$TM_{EF} = (TM/Al)_{sample}/(TM/Al)_{PAAS} \quad (2)$$

5.3. Strontium isotopes

Sr purification was performed according to the procedure described by Frei et al. (2011) and Fernandes et al. (2025a). 10 mL of the same solutions prepared for trace element analysis were dried down on a hotplate and redissolved in 1 mL of 3 M HNO_3. These solutions were then introduced into 1 mL columns containing 300 μL of SrSpec™ (Eichrome Inc./Tristchem) resin (50–100 mesh). The columns were

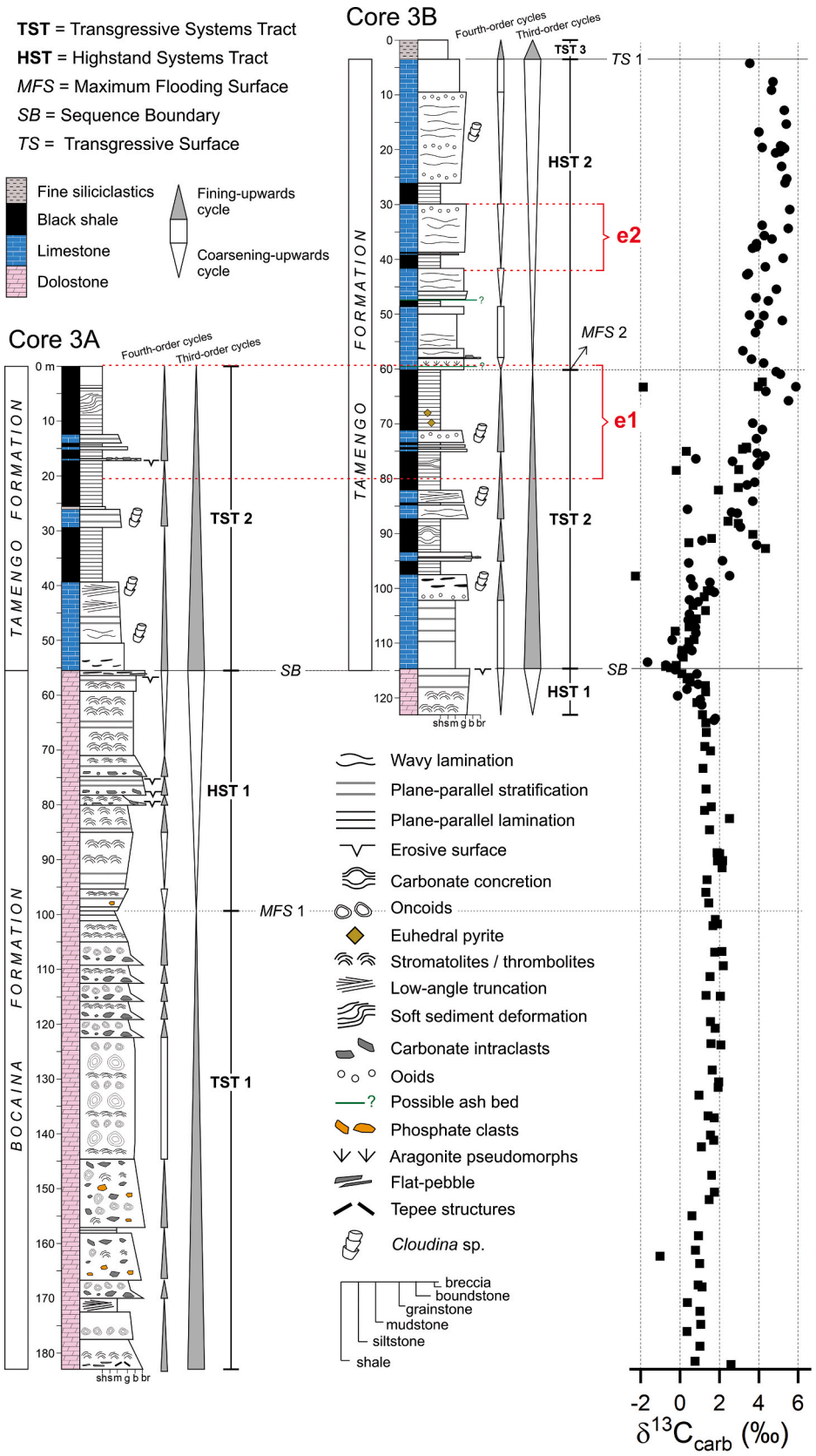

Fig. 2. Stratigraphic columns of GRIND-ECT cores 3A and 3B with sequence stratigraphic interpretation and $\delta^{13}C$ profiles (after Fernandes et al., 2025b). Squares indicate samples from core 3A and circles, from core 3B. Zones e1 and e2 denote intervals with anomalous geochemical signatures within the Tamengo Formation.

calibrated through successive steps of ultra-pure water and 3 M HNO_3 addition. Matrix was eluted through twelve flushing steps of 1 mL of 3 M HNO_3. Then, the Sr was collected with ultra-pure water. Subsequently, samples were loaded onto outgassed 99.9 % single-Re filaments using a loading solution of 2.5 μL Ta_2O_5-H_3PO_4-HF on a VG sector 54 IT Thermal Ionization Mass Spectrometer (TIMS) at the University of Copenhagen. Analyzes for the NIST 987 Sr standard prepared in the same way as the samples yielded $^{87}Sr/^{86}Sr$ ratios of 0.710238 ± 0.000018 (2σ) (Fernandes et al., 2025a). The average long-term reproducibility for the analyzed samples was ± 0.000015 (2σ).

5.4. Cadmium isotopes

The method for Cd purification via chromatography followed the procedure described by Frederiksen et al. (2022a, 2024) and Fernandes et al. (2025a). Approximately 2 – 8 g of powdered sample (depending on the Cd concentration previously obtained via ICP-MS) was digested in a mixture of 0.5 M HNO_3/0.2 M HBr, with each 2 g of sample digested in 40 mL of mixture in a centrifuge tube. A $^{106}Cd/^{108}Cd$ double spike was added to the solutions, aiming to achieve the $^{106}Cd/^{110}Cd$ ratio of 0.5 ± 0.1 in the sample-spike mixture. Subsequently, the samples were centrifuged, and the supernatant was separated for the first chromatographic step. In this stage, we used 10 mL BioRad™ columns with AG-1X8 100–200 mesh anion resin. Matrix was eluted after successive addition of 0.5 M HNO_3/0.2 M HBr, 0.03 M HNO_3/0.2 M HBr, and 1 M HCl. The recovered solution during this matrix elution step was further processed for Cr separation. The second chromatographic step was performed using 1 mL disposable pipette tip columns, and matrix was eluted in the same way as the first step. Cd was collected using 0.25 M HNO_3 in Savillex™ Teflon beakers.

Samples were loaded onto outgassed single-Re filaments using 2.5 μL of an 8:1:1 mixture of silicic acid, 1 M phosphoric acid, and saturated boric acid. The isotopic measurements were conducted in an IsoProbe-T TIMS at the University of Copenhagen. ^{112}Cd beam intensities were between 150 and 600 mV, depending on the quality of the signal. Details of mass spectrometric runs of Cd are presented in a recent publication by Frei et al. (2024). Results are expressed using the delta (δ) notation in per-mil (‰) with respect to the NIST 3108 reference material.

$$\delta^{114}Cd(‰) = \left[\left(^{114}Cd/^{110}Cd_{sample}/^{114}Cd/^{110}Cd_{NIST3108}\right) - 1\right] \times 10^3 \quad (3)$$

The results of runs of the NIST 3108 through analyses at ^{110}Cd beams of 300, 600, and 1000 mV yielded the long-term $\delta^{114}Cd$ of 0.00 ± 0.10 ‰ (2σ, n = 120) (Fernandes et al., 2025a). Additionally, analyses of "Münster Cadmium" (MCd) and BAMIO12 reference solutions yielded $\delta^{114}Cd$ values of +4.56 ± 0.75 ‰ (2σ, n = 4) and −1.37 ± 0.07 ‰ (2σ, n = 4), respectively (Fernandes et al., 2025a). These values agree with the values obtained by other laboratories (Abouchami et al., 2013).

5.5. Chromium isotopes

The method for Cr purification followed the procedure described by Frei et al. (2011) and Gilleaudeau et al. (2016). A ^{50}Cr-^{54}Cr double-spike (Schoenberg et al., 2008) was added to powdered samples with a 4:1 sample:spike volume ratio. 4 mL of *aqua regia* was added to the solution collected after the first Cd purification step to remove the Br from solution. Samples were then dried down on a hotplate and redissolved in 20 mL 0.1 M HCl. 1 mL of 1 M $(NH_4)S_2O_8$ was added as an oxidant activator. Beakers were subsequently placed on a hotplate for 90 min at 130 °C to oxidize all the Cr(III) to Cr(VI). Cr purification followed two ion exchange steps. The first chromatographic step was performed using anion exchange columns charged with 2 mL of AG 1X8 100–200 mesh resin. Matrix was eluted through successive flushing steps of ultra-pure water and 6 M HNO_3, and Cr was collected using 6 mL of 2 M HNO_3 and 330 μL of 5 % H_2O_2. The second step was performed with a cation exchange column charged with an AG-50 W-8 200–400 mesh resin. Dried samples from the anion column separation were re-dissolved in 200 μL of 6 M HCl, then diluted with 2 mL ultra-pure water and passed over the cation columns.

Samples were loaded onto outgassed single-Re filaments using the same loading solution as for the Cd procedure. Isotopic measurements were carried out with an IsotopX *Phoenix* TIMS at the University of Copenhagen. Analytical details were presented by Frei et al. (2024). Results of Cr isotope compositions are also reported using the delta notation in per-mil, with respect to the "zero-delta" NIST 979 reference material.

$$\delta^{53}Cr(‰) = \left[\left(^{53}Cr/^{52}Cr_{sample}/^{53}Cr/^{52}Cr_{NIST979}\right) - 1\right] \times 10^3 \quad (4)$$

Analyses of the NIST 979 material prepared using the same procedure as the samples yielded $\delta^{53}Cr$ = 0.06 ± 0.09 ‰ (n = 125, 2σ) (Fernandes et al., 2025a).

6. Results

6.1. Elemental geochemistry

Elemental geochemical data is provided in the Supplementary Data (Table S1). Mg/Ca ratios present a clear decreasing pattern, from 0.53 in the Bocaina Formation to less than 0.01 in the Tamengo Formation (Fig. 3), as is expected from the main mineralogy of these units, passing from dolomites to limestones. Notably, samples in the lowermost Tamengo Formation present intermediate Mg/Ca ratios, consistent with dolomitic limestones. Th/U ratios are relatively high in the lower Bocaina Formation, spanning from 1.25 to 5.43, and decrease upwards down to 0.38. In the Tamengo Formation, Th/U ratios are lower, down to 0.23, apart from intervals e1 and e2 (Fig. 3b), when Th/U peak up to 7.78. An opposite pattern is observed in U_{EF} and V_{EF} plots, with low values in the Bocaina Formation and intervals e1/e2 (around 50 for U_{EF} and 4 for V_{EF}) and high values in the Tamengo Formation, apart from intervals e1/e2, up to 1054 and 15, respectively (Fig. 3B).

Al abundances are relatively low throughout the whole succession, varying from 37 to 433 mg/kg, with two peaks in intervals e1 and e2, up to 1527 mg/kg. Fe concentrations vary around 1300 mg/kg in the Bocaina Formation and 400 mg/kg in the Tamengo Formation, where intervals e1 and e2 also present a peak up to 4912 mg/kg. Mn/Al ratios vary from 0.2 to 5.0 and peak up to 35.8 in interval e1. P abundances range from 64 to 806 mg/kg in the Bocaina Formation and from 33 to 603 mg/kg in the Tamengo Formation, with two peaks during e1/e2 up to 1042 mg/kg and in the uppermost sample of core 3B of 1277 mg/kg. Mn/Sr ratios span from 0.01 to 3.15, with high values (>2) during interval e1 and at the Bocaina-Tamengo limit.

The rare earth elements and yttrium (REY) concentrations obtained for the Bocaina and Tamengo Formations reveal a prominent MREE enrichment with respect to LREE and heavy rare earth elements (HREE). This enrichment results in a MREE-bulge pattern in the distribution diagram (Fig. 4) and elevated $(Dy/Sm)_n$ ratios, up to 1.55. PAAS-normalized Ce anomalies range from 0.94 to 1.27, with a clear increase from the Bocaina to the Tamengo formations (Fig. 3).

6.2. Isotope geochemistry

All isotope results are listed in the Supplementary Data (Table S2). The $^{87}Sr/^{86}Sr$ values in the Bocaina Formation show a consistent trend around 0.7100, with a few values up to 0.7118 close to the Bocaina-Tamengo transition (Fig. 5). Samples from the Tamengo Formation also present elevated values close to the contact, up to 0.7119. The main trend in the Tamengo Formation displays $^{87}Sr/^{86}Sr$ values slowly dropping from 0.7095 down to 0.7084. This minimum value is reached around 20 m depth of core 3B, above which the $^{87}Sr/^{86}Sr$ curve presents a slight increase back to 0.7085.

The average $\delta^{53}Cr_{raw}$ in the Bocaina Formation is −0.26 ± 0.32 ‰

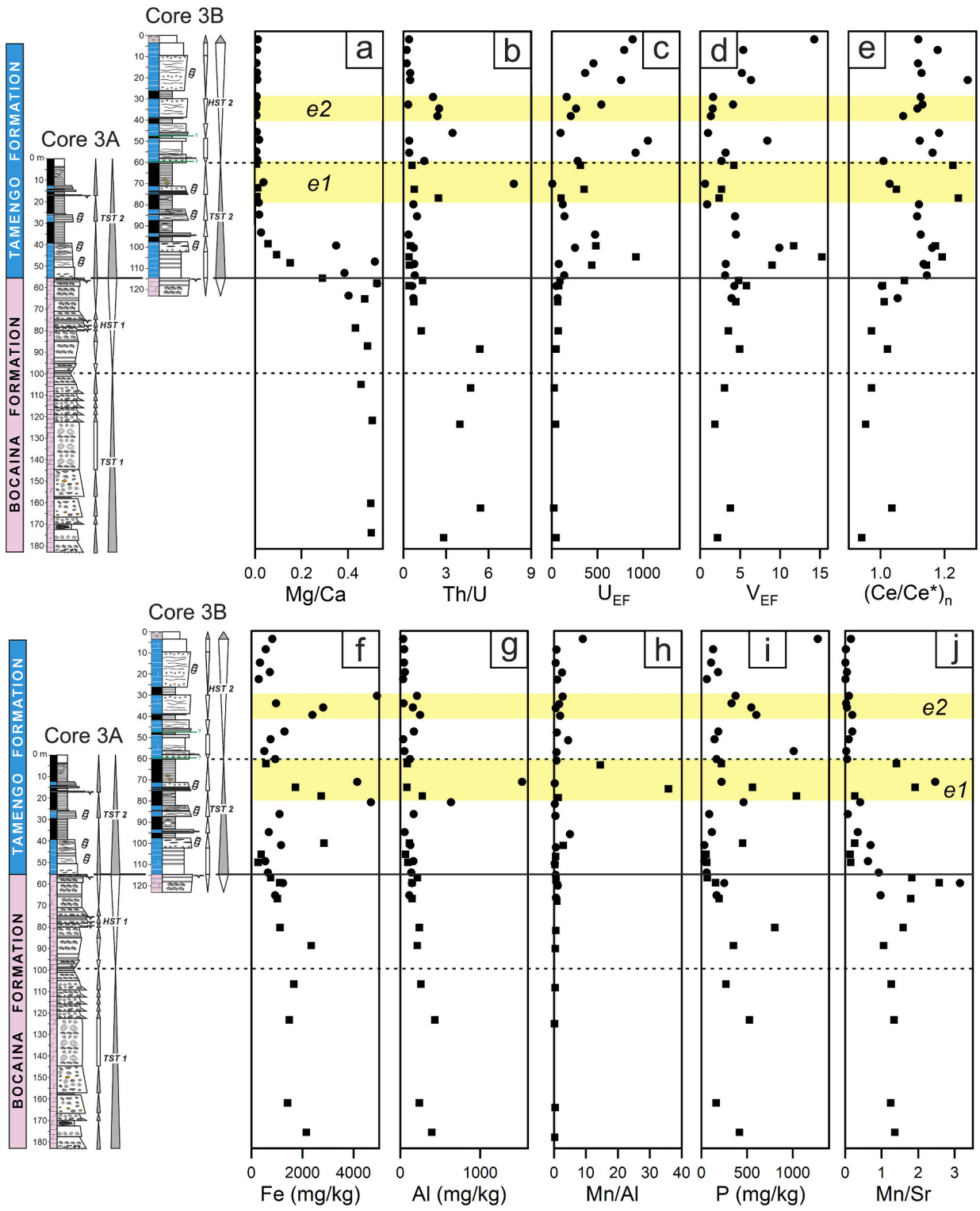

Fig. 3. Elemental plots along with the stratigraphic columns of cores 3A and 3B. Yellow fields e1 and e2 denote intervals with relatively high Al, Fe, Mn/Al, and P, as well as anomalous isotopic signatures in the Cr-Cd record (see Fig. 5). Squares indicate samples from core 3A and circles represent samples from core 3B. Data is provided in the Supplementary Data (Table S1).

(2σ, n = 10), presenting a relatively homogeneous distribution throughout the unit (Fig. 5). Only one sample yielded a positive value, of +0.04 ‰. In the Tamengo Formation, the average $\delta^{53}Cr_{raw}$ is +0.20 ± 0.54 ‰ (2σ, n = 18), showing a plateau around + 0.4 ‰ with two brief negative excursions (e1 and e2) towards negative values, around −0.2 ‰, at 75 m and 35 m depth of core 3B (Fig. 5).

The $\delta^{114}Cd_{raw}$ data presented an average of −0.02 ± 0.40 ‰ (2σ, n = 10) in the Bocaina Formation and −0.13 ± 0.52 ‰ (2σ, n = 9) in the Tamengo Formation (Fig. 5). Positive values are exclusively found in the upper Bocaina Formation, in the transgressive systems tract of this unit, from 55 to 105 m depth of core 3A. In the Tamengo Formation, negative $\delta^{114}Cd_{raw}$ values were obtained at depths coincident with e1 and e2.

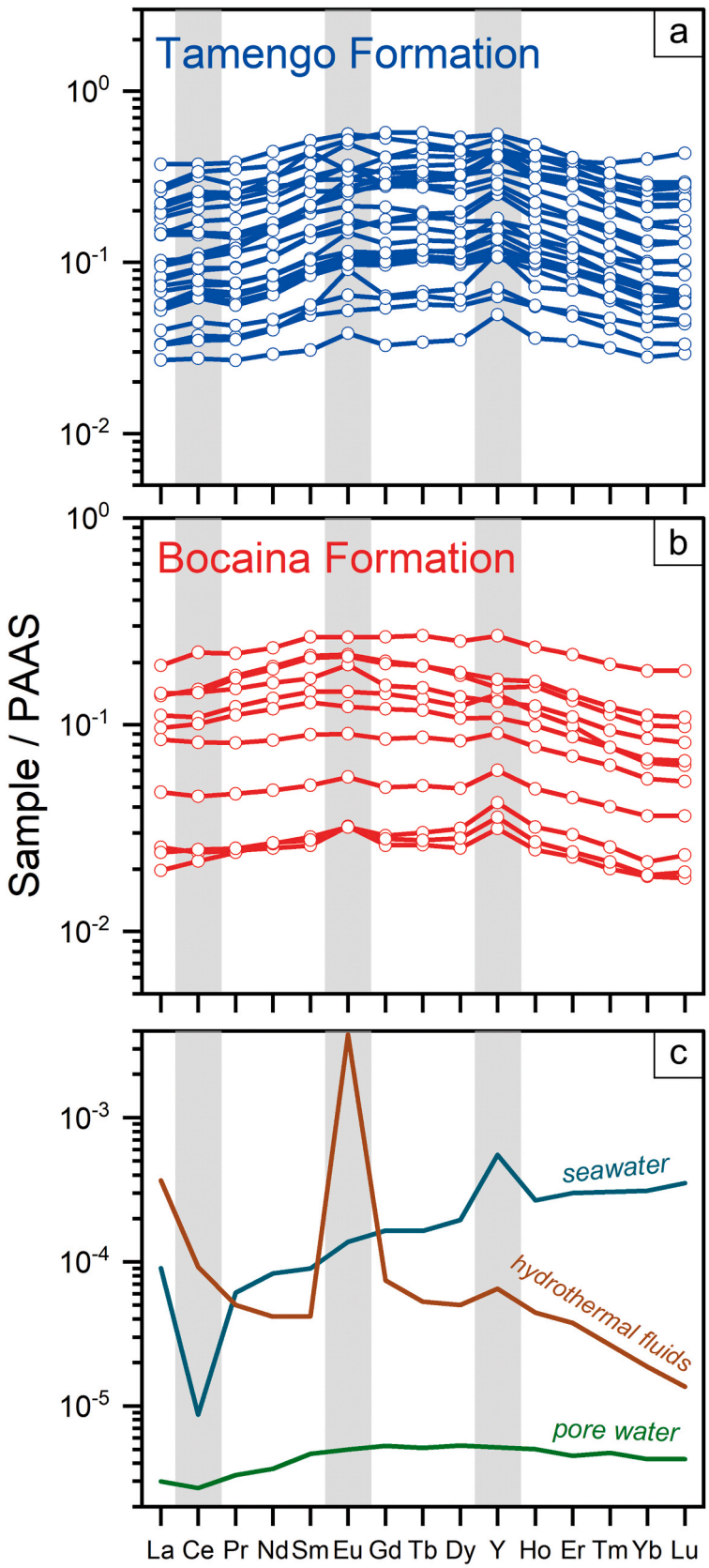

Fig. 4. PAAS-normalized REE and Y distribution obtained in the Bocaina (a) and Tamengo (b) formations. Modern seawater, high-T hydrothermal fluids (Douville et al., 2002), and Fe-rich marine pore waters (Haley et al., 2004) REY distributions are plotted for comparison in (c).

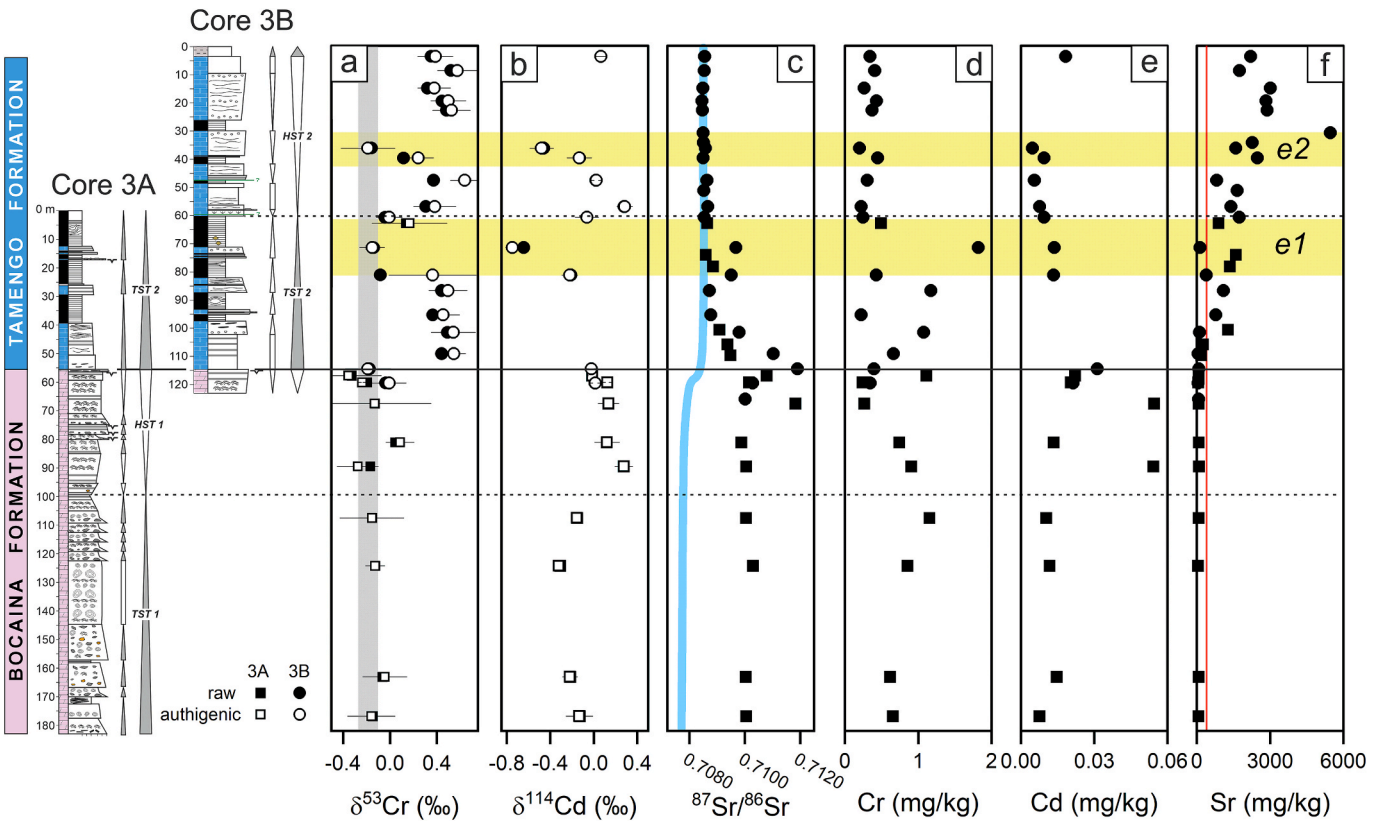

Fig. 5. (a) $\delta^{53}Cr$, (b) $\delta^{114}Cd$, (c) $^{87}Sr/^{86}Sr$, (d) Cr, (e) Cd, and (f) Sr plots along with columnar sections of cores 3A and 3B. Error bars denote 2σ in the Cr and Cd plots. The gray area in (a) represents the range of BSE values (Schoenberg et al., 2008), the blue area in (c) corresponds to the late Ediacaran global seawater trend (Chen et al., 2022), and the red vertical line in (f) denotes the [Sr] cutoff value of 400 mg/kg of samples with altered $^{87}Sr/^{86}Sr$ values (see text for details). Data is given in the Supplementary Data (Table S2).

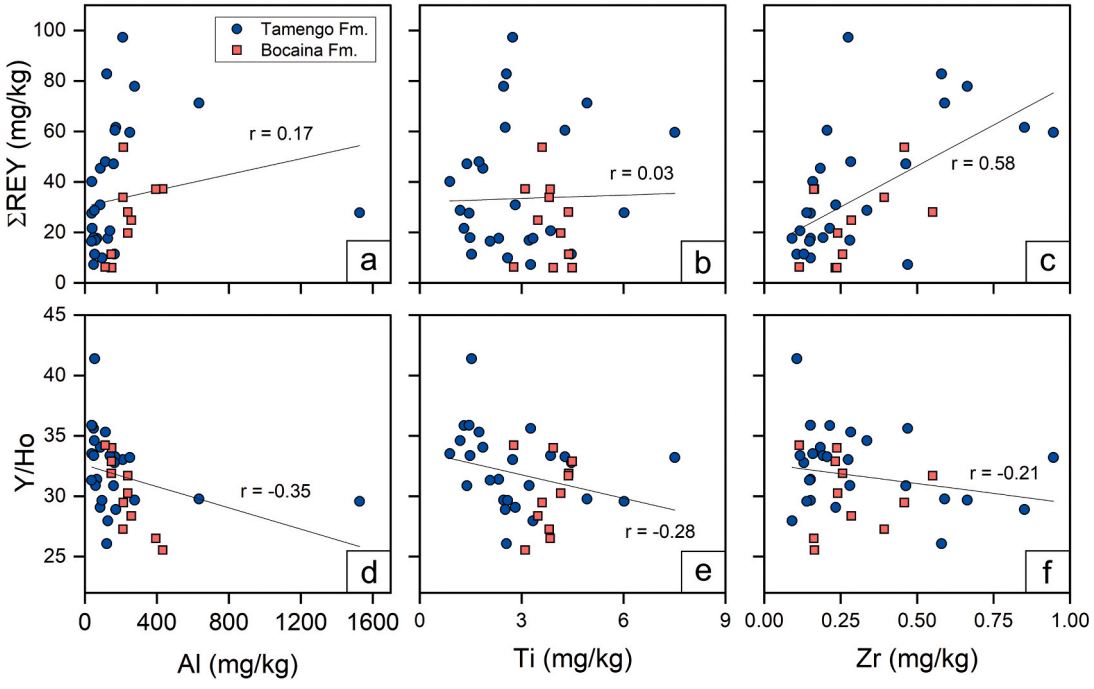

Fig. 6. Cross-plots of Al, Ti, and Zr versus ∑REY and Y/Ho.

7. Discussion

7.1. Effects of detrital contamination on REY patterns

The REY pattern of carbonates can be subject to intense alteration of the marine signal by detrital contaminants, as detrital particles typically have 10 to 100 times more REE than carbonate minerals (Nothdurft et al., 2004). Aluminum, titanium, and zirconium are frequently used as detrital indicators, due to their relative immobility in solution and resistance during weathering. Y/Ho ratios and ∑REY in our samples do not significantly correlate with Al and Ti (Fig. 6), indicating that the detrital contamination from clayey fractions on the REY pattern was negligible. A significant correlation, however, was observed in the Zr versus ∑REY plot (Fig. 6c), suggesting that REY enrichment may have been caused by contamination from sand-size detrital fractions. Nevertheless, given the lack of significant correlation between Zr and Y/Ho and that all samples, even the ones with high Zr, present superchondritic Y/Ho ratios (>25), it is unlikely that this enrichment affected the shape of the REY distribution, as high amounts of detrital phases often obliterate this positive Y anomaly (Nothdurft et al., 2004; Gong et al., 2021).

7.2. Origin of REY patterns and seawater redox-stratification

The REY distribution in modern ocean waters follows the so-called "seawater signal", presenting a positive La anomaly, negative Ce anomaly, minor positive Gd anomaly, LREE depletion, and superchondritic Y/Ho ratios (Zhang and Nozaki, 1996; Nozaki et al., 1997). Ancient carbonates can record the pristine REY signature of the seawater from which they are formed, giving valuable information regarding trace elements remobilization and redox conditions through the magnitude of Ce anomalies (German and Elderfield, 1990; Tostevin et al., 2016a). Nevertheless, early diagenetic processes can significantly alter the original REY distribution, especially under anoxic pore water environments (Zhang and Shields, 2023).

The samples analyzed here present a clear MREE-bulge pattern, easily verified in the distribution diagrams (Fig. 4) and through the relatively high Dy/Sm ratios. Similar results were obtained in previous studies on the Tamengo Formation from Corumbá (Spangenberg et al., 2014) and Serra da Bodoquena (Fernandes et al., 2024) areas. Such MREE-bulge patterns can be formed during precipitation of authigenic phosphate (Bryne et al., 1996; Shields and Stille, 2001; Pattan et al., 2005), REY complexation with organic matter (Tang and Johannesson, 2010), and remobilization of REY after reduction of Fe-Mn oxyhydroxides in anoxic diagenetic environment (de Baar et al., 1985; Haley et al., 2004; Paul et al., 2019). There is no significant correlation between P and Dy/Sm (Fig. 7), suggesting that phosphate authigenesis was not a driver for these MREE-bulge patterns. Furthermore, organic matter has about 10 times less REE than Fe-Mn nodules (Freslon et al., 2014), making it, if at all, a minor driver for the widespread MREE enrichments observed in carbonate rocks of the Corumbá Group.

Conversely, redox-stratified water column and ferruginous conditions are attributed to the Tamengo Formation based on iron speciation data (Caxito et al., 2024), and significant positive correlations obtained between Mn/Al (and Fe/Al) and Dy/Sm (Fig. 6d) reinforce the interpretation of Fe-Mn oxyhydroxides as the main MREE driver. In this case, Fe-Mn oxyhydroxides formed in the oxic layer preferentially incorporate MREE relative to LREE and HREE (Sholkovitz et al., 1994), as well as Ce (VI) relative to other REE (Bau and Koschinsky, 2009; de Baar et al., 2018). Subsequently, in an anoxic pore water environment, dissolution of these Fe-Mn oxyhydroxides and REY remobilization take place, causing the REY signal of carbonate rocks to be overprinted and forming the MREE-bulge pattern (Haley et al., 2004). Therefore, the obtained REE patterns probably represent an early diagenetic remobilization in an anoxic pore water environment. Interestingly, Ce anomalies increase from around 1.0 (no anomaly) in the Bocaina Formation to ca. 1.2 in the Tamengo Formation, which potentially demonstrates that diagenetic processes in the Tamengo Formation took place in the Mn reduction zone, where the dissolution of Mn-oxyhydroxides release Ce (German et al., 1991; Ling et al., 2013). This possibly suggests that the redoxcline was shallower in the Bocaina Formation compared to the Tamengo Formation, given that the dissolution of Mn-particulate released relatively more Ce in the Tamengo Formation.

7.3. Element geochemical proxies

Uranium (U) and vanadium (V) are redox-sensitive elements. Their abundances in sedimentary rocks have the potential to track changes in past seawater redox conditions (Emerson and Huested, 1991). Under oxygenated conditions, U is mainly found as U(VI) in highly soluble carbonate complexes and V is present as V(V) in oxyanions. Under anoxic seawater, both U and V are removed from the water column by anoxic sediments and insoluble oxyhydroxides (Tribovillard et al., 2006). U and V enrichment factors (EFs) are widely used as seawater redox proxies in ancient sedimentary rocks. In contrast, thorium (Th) is not significantly affected by redox shifts and remains insoluble in the water column, rendering Th/U ratio in carbonates to be a reliable paleoredox proxy for tracking ocean redox conditions (Marenco et al., 2016). As presented in the previous section, both units likely presented a sustained anoxic pore water environment, which limited U and V remobilization, therefore recording water-column redox conditions. The U_{EF}, V_{EF}, and Th/U data of our samples show clear changes in redox conditions throughout the Bocaina and Tamengo formations (Fig. 3). Relatively high values of Th/U (>2) coupled with low values of U_{EF} and V_{EF} (<200 and <5, respectively) in the Bocaina Formation and intervals e1/e2 indicate that these were periods of expanded anoxia, with lower dissolved U and V in the water column. In contrast, the Tamengo Formation, excluding intervals e1/e2, presents the opposite pattern, likely indicating increased oxia. This further supports that the redoxcline was

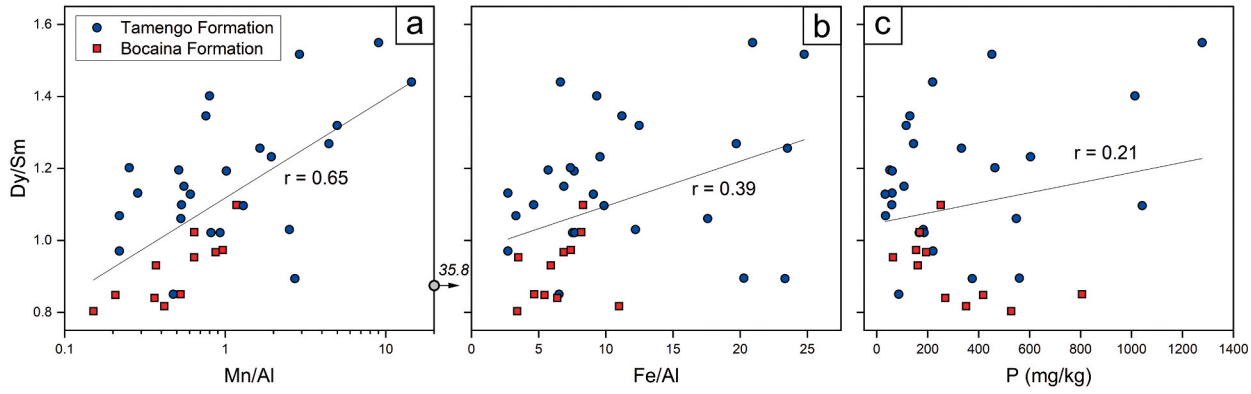

Fig. 7. Plots of Mn/Al (a), Fe/Al (b), and P (c) versus Dy/Smr for the studied samples. Only (a) and (b) yielded significant correlations (i.e., $p < \alpha = 0.01$).

deeper in the Tamengo Formation (outside the e-intervals) compared to the Bocaina Formation.

Phosphorus (P) is the ultimate limiting nutrient in the ocean in geological timescales. P abundances in carbonate rocks can be applied as a paleoproductivity proxy, although some observations regarding P remobilization during diagenesis and the link between P cycling and redox conditions challenge this application (Tribovillard et al., 2006). Similarly to the other proxies discussed in this section, P concentrations are relatively high during e1 and e2, suggesting increased primary productivity during these intervals (Fig. 3). P abundances are also relatively high in some samples from the Bocaina Formation, up to 806 mg/kg. Notably, the Bocaina Formation in cores 3A and 3B does not present phosphorite layers, in contrast to the widespread phosphorite beds in the Serra da Bodoquena region, mostly associated with reef stromatolites (Hippertt et al., 2023). This contrast suggests different productivity levels in the lagoonal and reef/rim environments, if phosphorite deposition was driven by upwelling. Alternatively, these overall high P concentrations in the lagoonal setting of the Bocaina Formation may derive from P-bearing detrital materials or authigenic phases unrelated to upwelling.

Considering the points listed above, the Bocaina Formation and intervals e1 and e2 within the Tamengo Formation display increased anoxia, detrital input, and primary productivity. Conversely, the Tamengo Formation, outside e1 and e2, probably had a deeper redoxcline and low productivity levels. The links between these parameters and the isotope data will be further explored in the next sections.

7.4. Variations of $^{87}Sr/^{86}Sr$ values

In the seawater, the strontium (Sr) isotope composition is modulated by the mixture of Sr derived from two major sources: more radiogenic (i.e., ^{87}Sr-enriched) Sr from continental weathering and less radiogenic (i.e., ^{87}Sr-depleted) Sr from the oceanic lithosphere (Asmerom et al., 1991; Richter et al., 1992). Carbonate minerals record the $^{87}Sr/^{86}Sr$ signature of the seawater from which they are formed and therefore act as archives for reconstructing the paleo-seawater $^{87}Sr/^{86}Sr$ curve (Shields, 2007; Halverson et al., 2010; Zhou et al., 2020). It is known that the $^{87}Sr/^{86}Sr$ curve presents relatively high values in the late Ediacaran, around 0.7085 (Kaufman et al., 1993; Halverson et al., 2010), which is attributed to the formation of collisional orogens during the amalgamation of Gondwana (Asmerom et al., 1991; Shields, 2007; Cordani et al., 2020) or to protracted effects of Rodinia break-up (Halverson et al., 2007). The data obtained here for the Corumbá Group reveals two distinct patterns of Sr isotopes. Firstly, in the Bocaina Formation, the $^{87}Sr/^{86}Sr$ values are consistent around 0.7100 and increase to 0.7118 close to the contact with the Tamengo Formation. Secondly, in the Tamengo Formation, the $^{87}Sr/^{86}Sr$ values drop from ca. 0.7090 to 0.7085 (Fig. 5).

It is noteworthy that all samples from the Bocaina Formation correspond to Sr-depleted dolostones, with Sr concentrations lower than 85 mg/kg. Similarly, dolomitic limestone samples from the lowermost Tamengo Formation that exhibit high $^{87}Sr/^{86}Sr$ values also present low Sr concentrations, usually lower than 300 mg/kg. Significant negative correlations were obtained between $^{87}Sr/^{86}Sr$ and Sr concentrations (exponential) and Mg/Ca (linear) (Fig. 8a and b), which further supports that the radiogenic $^{87}Sr/^{86}Sr$ signal was obtained exclusively from Sr-depleted dolostones and dolomitic limestones. These Sr-poor rocks are more susceptible to diagenetic $^{87}Sr/^{86}Sr$ overprint. A tentative cutoff value of [Sr] = 250 mg/kg has been applied in previous studies as a threshold between altered and unaltered samples (Halverson et al., 2007). Our data show a sharp increase of $^{87}Sr/^{86}Sr$ in samples with Sr

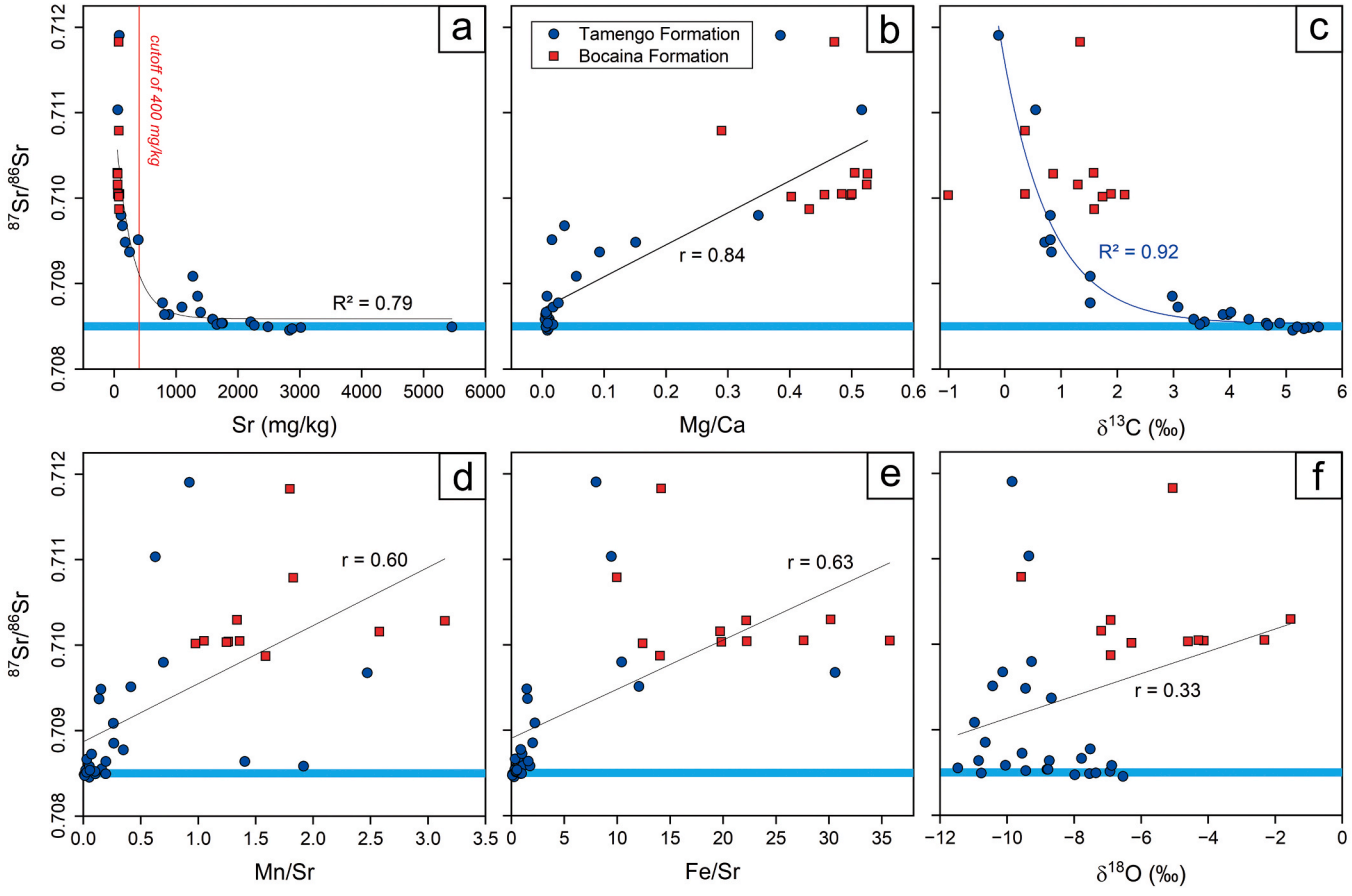

Fig. 8. Plots of Sr (a), Mg/Ca (b), $\delta^{13}C$ (c), Mn/Sr (d), Fe/Sr (e), and $\delta^{18}O$ (f) versus $^{87}Sr/^{86}Sr$ for the studied samples. Carbon and oxygen isotope data are from Fernandes et al. (2025b). The blue field denotes the assumed late Ediacaran seawater $^{87}Sr/^{86}Sr$ range.

abundances below 400 mg/kg, so we applied this value as cutoff (Fig. 8a). Therefore, in the case of the Bocaina Formation, the Sr isotope composition has been completely overprinted during post-depositional diagenesis and does not provide information regarding the connectedness of the basin with the open ocean.

In contrast, the $^{87}Sr/^{86}Sr$ values in the Tamengo Formation decrease down to 0.7085, precisely the late Ediacaran seawater ratio, which indicates complete Sr exchange between basin and open ocean. Values around 0.7085 have also been reported for the Tamengo Formation from the Laginha and Saladeiro sections, in Corumbá, and from the Horii section, in the Serra da Bodoquena area (Babinski et al., 2008; Boggiani et al., 2010), showing that this signal is ubiquitous in this unit. Interestingly, a negative exponential correlation has been observed between $^{87}Sr/^{86}Sr$ and $\delta^{13}C$ for samples from the Tamengo Formation (Fig. 8c), which possibly suggests that the short-lived negative $\delta^{13}C$ excursion at the base of this unit may have a diagenetic origin. Significant correlations were also observed between $^{87}Sr/^{86}Sr$ and Fe/Sr, Mn/Sr, and $\delta^{18}O$, further indicating this diagenetic origin of the highest $^{87}Sr/^{86}Sr$ values (Fig. 8d–f).

7.5. Assessing the detrital and diagenetic influence on the Cr-Cd isotope record

Verifying the contribution of detrital Cr on the isotope data is vital to correct the obtained $\delta^{53}Cr_{raw}$ values and calculate the true authigenic signatures. The correction for detrital Cr in carbonate samples is performed via a four-step algorithm (Gilleaudeau et al., 2016; Rodler et al., 2016; Klaebe et al., 2021), which compares the Cr and Al concentrations of the sample with those of PAAS (McLennan, 1989). In this algorithm, it is assumed that the detrital chromium isotope composition ($\delta^{53}Cr_{det}$) is -0.12 ± 0.10 ‰, as this is the isotope composition of igneous and metamorphic rocks (Schoenberg et al., 2008), or Bulk Silicate Earth (BSE). The algorithm is:

$$[Cr]_{det} = [Cr]_{PAAS} \times \left([Al]_{sample} \Big/ [Al]_{PAAS} \right) \quad (5)$$

$$f_{det} = [Cr]_{det} / [Cr]_{sample} \quad (6)$$

$$f_{auth} = 1 - f_{det} \quad (7)$$

$$\delta^{53}Cr_{auth} = \left(\delta^{53}Cr_{raw} - \delta^{53}Cr_{det} \times f_{det} \right) / f_{auth} \quad (8)$$

where f_{det} and f_{auth} are the fraction of detrital and authigenic Cr in the sample, respectively. Importantly, we considered $[Cr]_{PAAS}$ to be 55 mg/kg, half of the value reported by McLennan (1989), as its concentration appears to be overestimated in its reference for detrital siliciclastic component corrections, which otherwise sometimes result in a fraction of detrital Cr above 100 %. In Eq. (8), the $\delta^{53}Cr_{raw}$ is the measured Cr isotope composition and the $\delta^{53}Cr_{auth}$ is the authigenic Cr isotope composition that is used for paleoenvironmental interpretations. Samples with high Al concentrations or with high f_{det} present $\delta^{53}Cr_{raw}$ in the range of $\delta^{53}Cr_{det}$ (Fig. 9). Therefore, in these samples, the detrital Cr predominated in the isotope composition, resulting in greater deviations of the $\delta^{53}Cr_{auth}$ compared to the $\delta^{53}Cr_{raw}$. Fortunately, only two samples yielded more than 40 % of detrital Cr, indicating a relatively pure dataset with respect to detrital Cr influence.

The same algorithm applied for Cd revealed negligible amounts of detrital Cd ($[Cd]_{det}$), which is expected for carbonates (Frederiksen et al., 2022a). In this case, as Cd is not reported for PAAS, we used the Cd concentration of average loess (0.12 mg/kg) and the Cd isotope composition of BSE ($\delta^{114}Cd_{det}$) of -0.06 ± 0.03 ‰ (Pickard et al., 2022). Only one sample yielded f_{det} above 5 %. Intriguingly, a weak correlation was obtained for Al versus $\delta^{114}Cd_{raw}$ (Fig. 9), and samples with higher Al and f_{det} present $\delta^{114}Cd_{raw}$ values below that of BSE, which suggests that

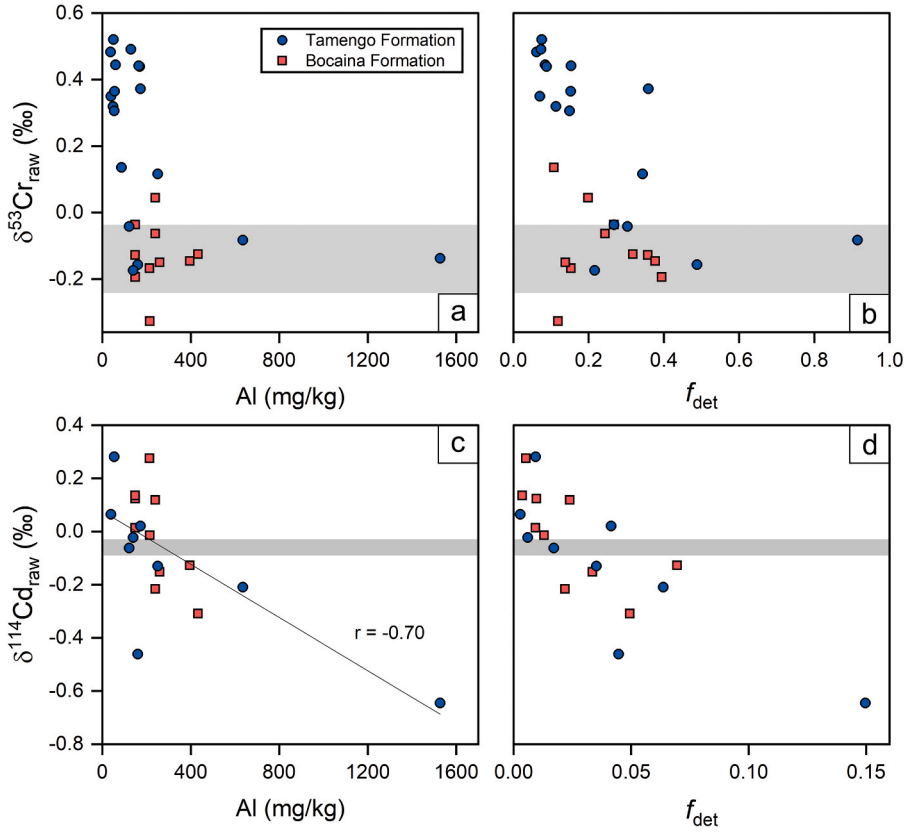

Fig. 9. Cross-plots of Al and fraction of detrital Cr (f_{det}) versus $\delta^{53}Cr_{raw}$. The gray areas correspond to the range of Bulk Silicate Earth $\delta^{53}Cr$ (Schoenberg et al., 2008) and $\delta^{114}Cd$ (Pickard et al., 2022).

Cd isotope composition roughly correlates with detrital input in the basin, but the Cd isotope measurements was not significantly influenced by detrital contaminants.

The diagenetic effects on the geochemical signature of cores 3A and 3B, as indicated by element ratios and C and O isotope signature, are minimal, with an overall preservation of the primary $\delta^{13}C_{carb}$ signal, apart from samples close to the Bocaina-Tamengo limit (Fernandes et al., 2025b). Mn/Sr ratios are relatively low (<2) in most samples, with higher values in the Bocaina Formation compared to the Tamengo Formation (Fig. 3). This difference probably reflects a variation in mineralogy, considering that dolomites are typically Sr-depleted compared to co-occurring calcites or aragonites (Swart, 2015), which can generate relatively high Mn/Sr ratios unrelated to diagenetic alterations. Furthermore, no significant correlation was obtained between Mn/Sr and $\delta^{53}Cr_{auth}$ or $\delta^{114}Cd_{auth}$ (Fig. 10). Similarly, no correlation was observed between these proxies and $\delta^{18}O_{carb}$, presented by Fernandes et al. (2025b), which is typically considered to be altered in Precambrian rocks.

7.6. $\delta^{53}Cr$ variations and redox shifts in the Corumbá basin

Considering that shortly after 800 Ma or earlier the atmosphere oxygen levels reached 0.5 % PAL or perhaps more (Och and Shields-Zhou, 2012; Alcott et al., 2019; Williams, et al., 2019; Zhang et al., 2021), enough to promote wide oxidation of Cr(III) to Cr(VI) in soils (Frei et al., 2009; Frei et al., 2014; Frei et al., 2017; Daines et al., 2017; Gilleaudeau et al., 2016; Canfield et al., 2018), a positive $\delta^{53}Cr_{auth}$ signal in marine sedimentary archives younger than 800 Ma is expected. Even so, several Ediacaran archives present low $\delta^{53}Cr_{auth}$ values, indicating dynamic redox conditions and complex processes controlling Cr isotopic fractionation (e.g. Frei et al., 2013; Frank et al., 2019; Wei et al., 2020; 2018; Xu et al., 2022; He et al., 2023). The $\delta^{53}Cr_{auth}$ data obtained herein for the Corumbá Group show two distinct patterns: first, a rather homogeneous distribution within the range of BSE in the Bocaina Formation, and second, positive values around +0.4 ‰ with short-lived negative excursions (e1 and e2) in the Tamengo Formation.

In modern redox-stratified lakes, often regarded as Proterozoic-analogues, Fe-Mn oxyhydroxides, formed above the redoxcline, non-quantitatively uptake Cr. This results in an isotopic shift from positively fractionated $\delta^{53}Cr$ values towards lower, BSE-like values for the authigenic particulate Cr (Janssen et al., 2022). Indeed, Fe is a well-known Cr reductant and can significantly remove Cr(VI) from solution, leading to substantial isotope fractionation (Døssing et al., 2011; Joe-Wong et al., 2021). Below the redoxcline, these oxyhydroxides undergo reduction, releasing Fe, Mn, and Cr into deep waters (Janssen et al., 2022). As a result, sediments may potentially exhibit $\delta^{53}Cr$ in the range of BSE despite being formed under a water column with positive $\delta^{53}Cr$ above the redoxcline. Given the redox-stratified water column attributed to the Bocaina Formation, we propose that a similar mechanism may have operated during the deposition of this unit. Therefore, a relatively shallow redoxcline would have promoted deposition of shallow-water carbonates with Cr isotope compositions falling within the range of BSE.

In contrast, samples from the Tamengo Formation, excluding those from intervals e1 and e2, yielded positive $\delta^{53}Cr_{auth}$ values around +0.4 ‰, in agreement with the range of modern seawater, riverine input, and other late Ediacaran shallow-water carbonate sequences (e.g., Caxito et al., 2018; Wei et al., 2020), which points to incorporation of land-derived heavy Cr isotope signatures into the carbonate minerals. As the Tamengo Formation also represents a redox-stratified setting (Spangenberg et al., 2014; Caxito et al., 2024; Fernandes et al., 2024), it probably had a deeper redoxcline, with a considerably wider shallow platform environment in which the above-mentioned Fe-Mn shuttle would likely not have operated in the depositional *locus* of cores 3A and 3B, which further supports the interpretation drawn from elemental proxies. This increased seater oxygenation was potentially driven by enhanced circulation and oceanic ventilation during transgression, allowing for further water column mixing (Duda et al., 2014).

Intervals e1 and e2 correspond to negative $\delta^{53}Cr_{auth}$ excursions in the Tamengo Formation, with a shift to BSE values. These intervals also present high Al, Fe, and Th/U ratios, as well as low U_{EF} and V_{EF}, indicating ferruginous conditions and enhanced detrital input, despite no pronounced changes in lithology. A pronounced increase in Fe delivery would significantly enhance Cr(VI) reduction by both $Fe(II)_{aq}$ and $Fe(II)/Fe(III)_{particulate}$ in the basin. Non-quantitative Cr reduction often causes $\delta^{53}Cr_{auth}$ in sediments to decrease toward the range of BSE (Bauer et al., 2018). Furthermore, once anoxic conditions reached shallow areas, the Fe-Mn shuttle would once again operate, potentially driving the $\delta^{53}Cr$ back to BSE values. This hypothesis also explains the peaks in Al and Fe throughout the e-intervals.

These two episodes of anomalous Fe-delivery into the Corumbá Basin may have been caused by changes in exposed weathering source on land. Banded iron formations (BIFs) from the Cryogenian Jacadigo Group occur spatially close to the Corumbá Group, and weathering of these units may have substantially enhanced Fe transport into the Corumbá Basin. As the Jacadigo BIFs have a relatively narrow and well-known $\delta^{53}Cr$ range around +1.00 ‰ (Árting et al., 2023; Frei et al., 2024), it is possible to estimate the operating fractionation factor during Cr reduction in intervals e1/e2 by subtracting this value from the minimum $\delta^{53}Cr_{auth}$ value during these excursions, which is −0.19 ‰. The so-estimated fractionation factor is 1.2 ‰, which agrees with the effective fractionation factor relative to Cr reduction by Fe(II) of 1.1 ± 0.2 ‰ (Bauer et al., 2018). In summary, the Cr isotope record in the Corumbá Basin tracks changes in the extent of shallow water oxygenated area, revealing dynamic redox conditions in time.

7.7. Reconstruction of paleo-seawater $\delta^{114}Cd$ and primary productivity levels in the Corumbá basin

Experimental investigations have demonstrated that the incorporation of Cd during marine calcite formation results in an isotope offset ($\Delta^{114}Cd_{carb\text{-}sw}$) of 0.45 ± 0.12 ‰ (Horner et al., 2011) that must be considered when reconstructing past seawater Cd isotope composition ($\delta^{114}Cd_{sw}$). A recent study showed that this deviation can be applied to modern carbonates to reconstruct present-day surface seawater $\delta^{114}Cd$ of the Atlantic Ocean (Frederiksen et al., 2022a). Thus, it is possible to obtain $\delta^{114}Cd_{sw}$ by applying the following relation:

$$\delta^{114}Cd_{sw} = \delta^{114}Cd_{raw} + \Delta^{114}Cd_{carb-sw} \quad (10)$$

The samples from the Corumbá Group yield a wide range of $\delta^{114}Cd_{sw}$, from −0.23 to + 0.69 ‰ (Fig. 11). In the Bocaina Formation, $\delta^{114}Cd_{sw}$ are relatively low in the transgressive systems tract and increase during the highstand systems tract (Fig. 5), suggesting that the vertical profile of seawater $\delta^{114}Cd$ was somewhat similar to the modern oceans, with productive surface waters ($\delta^{114}Cd_{sw} = \sim 0.7$ ‰) and unproductive deep waters ($\delta^{114}Cd_{sw} = \sim 0.2$ ‰). Furthermore, relatively high Cd concentrations, above 0.05 mg/kg, were only obtained in samples with high $\delta^{114}Cd$ at the highstand systems tract of the Bocaina Formation, while the rest of the samples presented low [Cd], usually below 0.02 mg/kg, reinforcing this overall low productivity scenario in the transgressive systems tract (Fig. 5).

In the Tamengo Formation, most $\delta^{114}Cd_{sw}$ values are compatible with modern deep ocean $\delta^{114}Cd$, suggesting overall low bioproductivity in the Corumbá Basin after 550 Ma. The lowermost values, that occur in intervals e1 and e2, are lower than the modern deep ocean and Bulk Silicate Earth (BSE) $\delta^{114}Cd$ ranges (Fig. 11). Intriguingly, these intervals display relatively high P, otherwise suggesting pronounced bioproductivity levels, which apparently contrasts with the Cd isotope results. Therefore, a more complex mechanism controlling the seawater Cd isotope composition in the Tamengo Formation during the e-excursions needs to be envisaged, as we explore below.

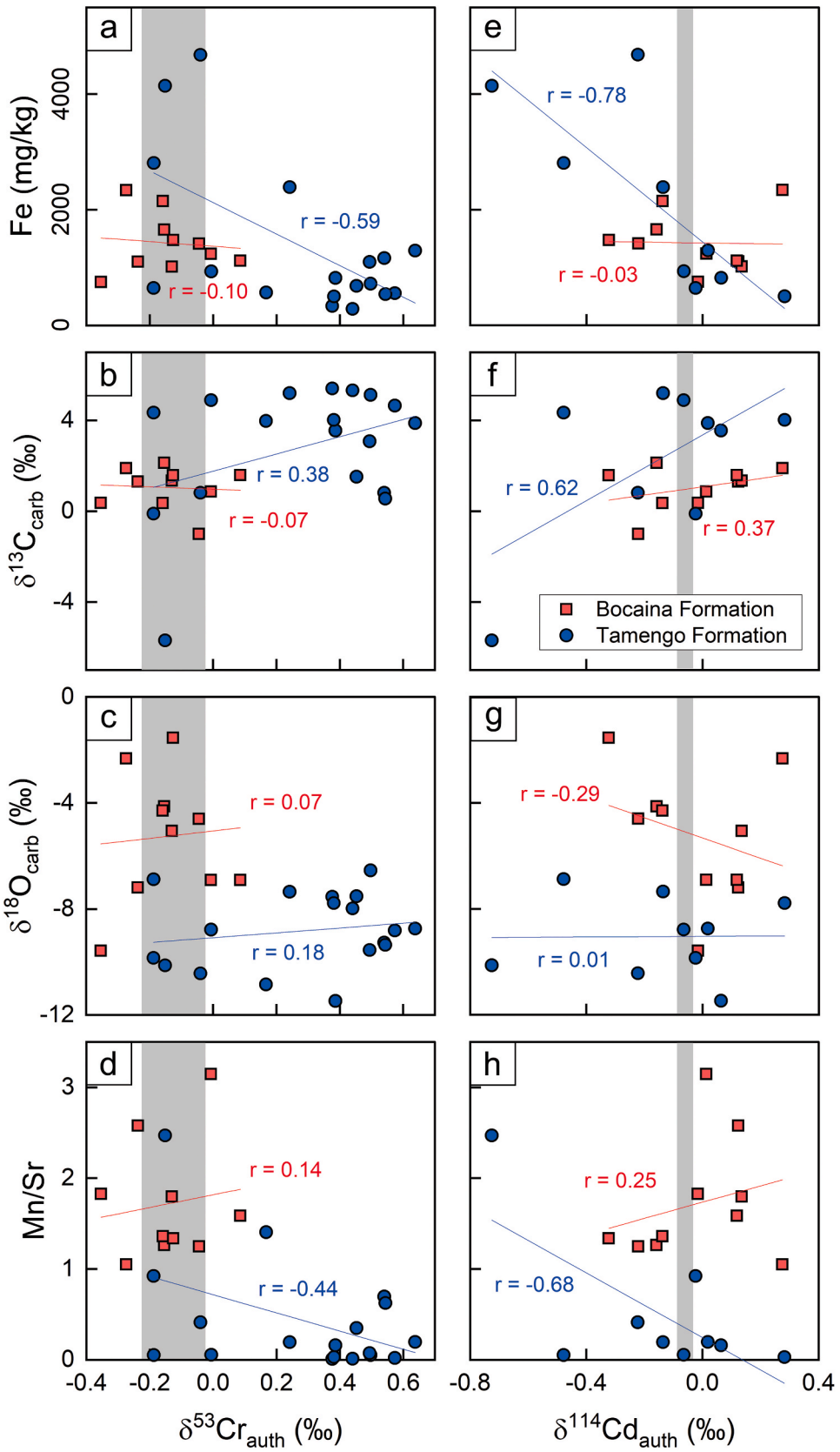

Fig. 10. Cross-plots of $\delta^{53}Cr_{auth}$ and $\delta^{114}Cd_{auth}$ versus Fe, $\delta^{13}C$, $\delta^{18}O$, and Mn/Sr. Carbon and oxygen isotope data are from Fernandes et al. (2025b). Gray vertical fields denote the range of BSE $\delta^{53}Cr$ (Schoenberg et al., 2008) and $\delta^{114}Cd$ (Pickard et al., 2022). Only the plot in (e), relative to the Tamengo Formation, yielded significant correlation (i.e., $p < \alpha = 0.01$).

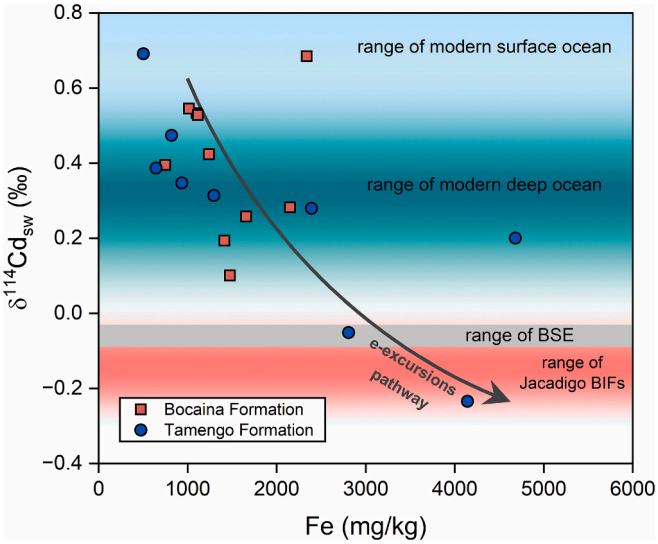

Fig. 11. Plot of Fe versus $\delta^{114}Cd_{sw}$ for samples from the Corumbá Group. Ranges of Bulk Silicate Earth (BSE) (Pickard et al., 2022), modern deep ocean, modern surface ocean (Sieber et al., 2023), and banded iron formations from the Jacadigo Group (Frei et al., 2024) $\delta^{114}Cd$ are indicated for comparison. Samples from the e-excursions present high Fe abundances and the lowest $\delta^{114}Cd_{sw}$ values.

In modern surface oceans, $\delta^{114}Cd_{sw}$ values are high due to preferential uptake of ^{110}Cd relative to ^{114}Cd by phytoplankton (Abouchami et al., 2011). However, if the demand for Cd exceeds the supply of it, phytoplankton cannot be selective, and Cd isotopes remain unfractionated within the organic cell relative to the average seawater composition (Druce et al., 2022). We propose that phytoplankton blooms under eutrophic conditions caused the overall low $\delta^{114}Cd_{sw}$ during e1 and e2. These eutrophication stages may have been caused by episodes of increased BIF weathering, as discussed previously, which could have fertilized the basin with Fe and other bio-essential elements. Indeed, studies demonstrate that the addition of micronutrients such as Fe, Co, and Zn significantly fuel microbial productivity in different trophic states (Dixon, 2008; Downs et al., 2008; Stoll et al., 2024). In our samples, Fe abundances significantly correlate with $\delta^{114}Cd$ (Fig. 9 and Fig. 11). Further, the input of isotopically light Cd into the basin would also have been higher, as BIFs from the Jacadigo Group have shown to be characterized by $\delta^{114}Cd$ from −0.23 to +0.01 ‰ (Frei et al., 2024), significantly lower than BSE values. The lowermost $\delta^{114}Cd$ values during the e-intervals fall within this range. The hypothetical scenario outlined above agrees with the expanded anoxia implied by paleoredox proxies in intervals e1 and e2. Notably, the e1 and e2 intervals also present an anomalous abundance of some acritarch microfossils from the genera *Leiosphaeridia* and *Germinosphaera* compared to under- and overlying strata, as shown by biostratigraphic data in Fernandes et al. (2025b). This observation may further support a profusion of photosynthetic organisms under eutrophic conditions. Interestingly, two coeval eutrophic intervals were previously attributed to the Tamengo Formation based on organic carbon and nitrogen isotope analyses in the Laginha section (Spangenberg et al., 2014). The detailed correlation of these intervals with the e-excursions are presented in the Supplementary Data (Fig. S1).

Our Cd isotope record for the Tamengo Formation (outside e1 and e2) is similar to the $\delta^{114}Cd$ record in the intra-shelf setting of the coeval late Ediacaran Dengying Formation (Yangtze Platform; Hohl et al., 2017; Frederiksen et al., 2022b), where water column mixing sustained a deeper redoxcline, enabled nutrient redistribution, and reduced productivity levels (Bowyer et al., 2017). In contrast, other studies, based on nitrogen and paired carbon isotopes, point to high productivity levels in the Ediacaran, particularly in basins influenced by strong upwelling (Gao et al., 2020; Ansari et al., 2023). Considering these local differences, it is safe to assume that local circulation and hydrodynamics impacted the extent of primary productivity in late Ediacaran basins, but under an overall low productivity scenario (Sperling and Stockey, 2018).

Furthermore, there is no significant correlation between $\delta^{114}Cd$ and $\delta^{13}C_{carb}$ (Fig. 10), which suggests that the carbon isotope record should not simply be explained by changes in primary productivity. Rather, it is probably a result of a complex interplay between productivity and organic matter preservation, which is in turn controlled by global-scale sea-level variations and water column redox conditions (Bowyer et al., 2024; Fernandes et al., 2025b). This hypothesis is further supported by the lack of a clear relationship between $\delta^{114}Cd$ and $\delta^{13}C_{carb}$ in other geologic settings and time periods (e.g., Frederiksen et al., 2024).

7.8. Paleoceanographic constraints in the Corumbá basin and implications for early animals' habitats

The data presented herein coupled with redox data compilation for the Corumbá Group (see Supplementary Data, Fig. S2 and Table S3) allows for the identification of two stages on the late Ediacaran carbonate sedimentation in the Corumbá Basin with respect to seawater circulation, redox setting, and trophic regime (Fig. 12). Firstly, the Bocaina Formation (ca. 565 –555 Ma) represents an oligotrophic, strongly redox-stratified basin, and with a very shallow redoxcline (Fig. 12a). Surface waters were characterized by modern-like high bioproductivity, while slightly deeper waters lacked significant primary production. In the reef setting, upwelling currents may have transported nutrients from bottom waters to lower depths, boosting bioproductivity and ultimately causing the deposition of extensive phosphorite layers within the reef rim (Hippertt et al., 2023; 2024). Unfortunately, our Sr isotope data was unconclusive regarding the connection of the Bocaina Formation with the open ocean. Secondly, the Tamengo Formation (ca. 550–540 Ma) represents a basin connected with the open ocean, presenting pronounced seawater circulation, and with a deeper and more dynamic redoxcline. During deposition of the Tamengo Formation sediments, ventilation and downwelling carried O_2-rich surface waters towards lower depths, increasing the oxygenated water volume of the basin under an oligotrophic regime (Fig. 12b), but still with anoxic bottom waters (Caxito et al., 2024). This scenario sporadically then may have changed due to episodes of high Fe-input (e-excursions), probably caused by weathering of the BIFs of the Jacadigo Group nearby (Fig. 1), which likely enhanced nutrient delivery into the basin and potentially fueled primary production (Fig. 12c).

The Bocaina and Tamengo formations also differ greatly with respect to their fossil content (Fig. 13 and compilation in the Supplementary Data, Fig. S2 and Table S4). The Bocaina Formation hosts a diverse assemblage of acantomorphic acritarchs (Gaucher et al., 2003; Morais et al., 2021) attributable to the Ediacaran Complex Acanthomorph Palynoflora, (ECAP; Grey et al., 2003; Grey, 2005) and putative metazoan micro-shells (Morais et al., 2024). In contrast, the microfossil content in the Tamengo Formation is less diverse yet more abundant (Morais et al., 2021; Fernandes et al., 2025b), with acritarchs attributable to the Late Ediacaran Leiosphere Palynoflora (LELP; Gaucher and Sprechmann, 2009). Occurrences of metazoan macrofossils are restricted to the Tamengo Formation, namely *Cloudina* sp., *Corumbella werneri*, and *Paraconularia ediacara* (e.g., Pacheco et al., 2018; Amorim et al., 2020; Leme et al., 2022; Osés et al., 2022; Afonso et al., 2024), while macrofossils are absent in the underlying Bocaina Formation. These differences in paleontological content between both units may be related to their distinct paleoceanographic scenario.

Several lines of evidence indicate that late Ediacaran communities were concentrated in shallow, high-energy, and dynamic environments that often experienced disturbances (Gehling and Droser, 2013; Meyer et al., 2014; Droser et al., 2017; Tarhan et al., 2018). This environmental preference is tightly linked to oxygen availability and exerted major controls on determining late Ediacaran metazoan distribution and even

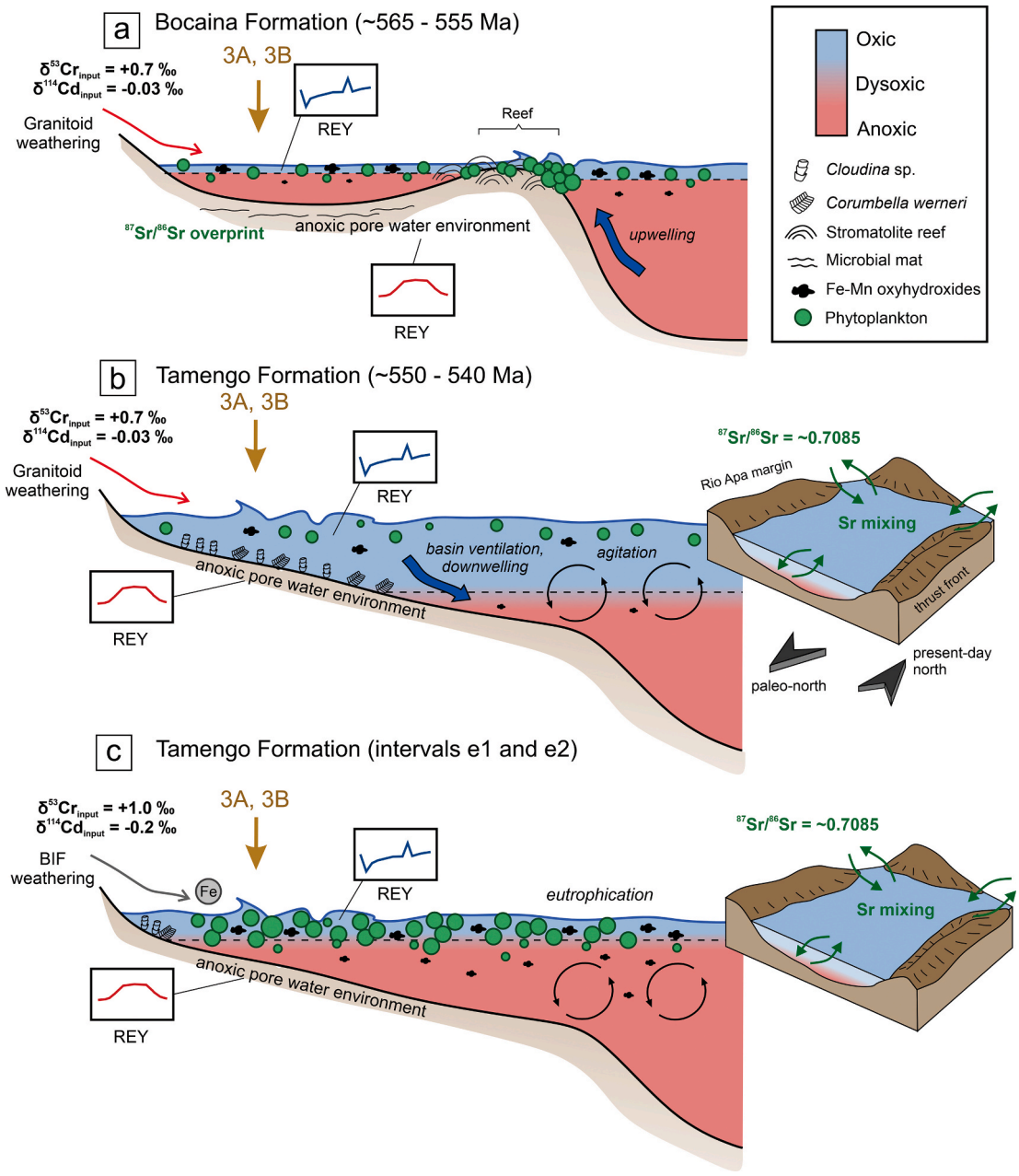

Fig. 12. Conceptual model of the operating REY (schematic PAAS-normalized diagrams), and Sr-Cr-Cd isotope systems during the deposition of the Bocaina (a) and Tamengo (b and c) formations. The yellow vertical arrow indicates the approximate location of cores 3A and 3B. In (a) and (b), the input value of $\delta^{53}Cr$ is the modern riverine average (D'Arcy et al., 2017) and the input $\delta^{114}Cd$ is the BSE value (Pickard et al., 2022). In (c), the input $\delta^{53}Cr$ and $\delta^{114}Cd$ values are the average values obtained from the Jacadigo BIFs (Árting et al., 2023; Frei et al., 2024). Note that widespread colonization of animals occurs only during (b), when oxygenated shallow water volumes are larger due to optimal circulation, productivity, and redox dynamics.

shaping these early animals' morphology (Bowyer et al., 2017; Droser et al., 2017; Evans et al., 2018). In the macrofossil-bearing Tamengo Formation, broad seawater circulation, water column mixing, and relatively low productivity levels for most of its depositional period led to surface water oxia under oligotrophic conditions, which became near-optimal habitats for early metazoans (except for intervals e1/e2, when eutrophication caused expanded anoxia). In contrast, low-oxygenated shallow basin waters prevailed during the deposition of the Bocaina Formation, which led to a predominantly anoxic environment and may partially explain the absence of animal macrofossils in this unit. Furthermore, within the Tamengo Formation, most *Cloudina*-bearing intervals reported by Fernandes et al. (2025b) from cores 3A and 3B are located outside e1 and e2, which may indicate that these eutrophic and ferruginous intervals were less ideal for *Cloudina* colonization and/or preservation.

Previous research points to elevated extinction rates during the White Sea–Nama transition (~550 Ma), likely driven by significant paleoenvironmental changes (Evans et al., 2022; Bowyer et al., 2024). Increasing marine anoxia is commonly invoked as the primary extinction driver during this interval. However, our results, along with previous studies (e.g., Bowyer et al., 2017; Liu et al., 2024), highlight that this final Ediacaran radiation occurred under both fluctuating redox conditions and in nutrient-limited settings. Specifically, the presence of an oligotrophic, food-limited environment in the Corumbá Basin, consistent with global patterns observed in the terminal Ediacaran oceans (Sperling and Stockey, 2018), suggests that both local redox

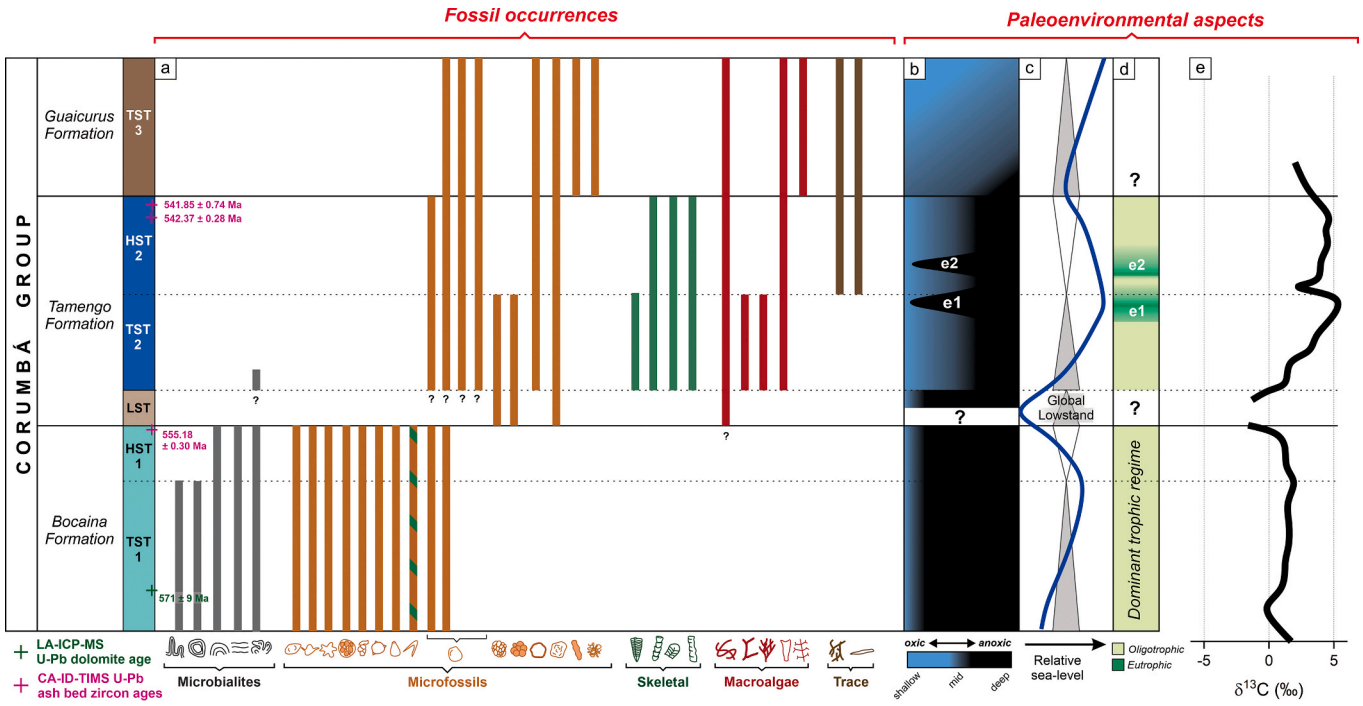

Fig. 13. Fossil occurrences (a) and paleoenvironmental evolution (b-e) of the upper Corumbá Group during the late Ediacaran. Redox data compilation is given in the Supplementary Data (Table S3). Fossil compilation with legend for symbols is given in Table S4. Sequence stratigraphy and carbon isotope curve after Fernandes et al. (2025b). Correlation of intervals e1 and e2 between Tamengo Formation sections is discussed in the Supplementary Data (Fig. S1). U-Pb zircon ages are from Parry et al. (2017) and U-Pb dolomite age is from Morais et al. (2024).

instability and widespread nutrient scarcity likely played critical roles in shaping the end-Ediacaran biosphere.

8. Conclusions

From the new elemental and isotope data presented herein for the late Ediacaran Corumbá Group, we draw the following conclusions:

(i) The REY patterns of the studied samples are compatible with early diagenetic REY remobilization in an anoxic pore water environment for both the Bocaina and Tamengo formations.
(ii) Elemental proxies point to relatively anoxic conditions in the Bocaina Formation and expanded oxia in surface waters of the Tamengo Formation, apart from intervals e1 and e2, when banded iron formation (BIF) weathering increased anoxia and boosted primary productivity.
(iii) The strontium isotope signature was completely overprinted during post-depositional diagenesis in the Bocaina Formation. In the Tamengo Formation, the $^{86}Sr/^{87}Sr$ values are consistent with the global seawater curve, revealing a hydrographic setting connected with the open ocean.
(iv) Chromium isotopes indicate redox shifts in the Corumbá Basin. The Bocaina Formation sustained predominantly anoxic conditions, while the overlying Tamengo Formation presents more oxygenated conditions, with a deeper redoxcline and water column mixing. The water column shifted back to predominantly anoxic during intervals e1 and e2.
(v) The cadmium isotope composition of the Bocaina Formation reveals productive surface waters and unproductive slightly deep waters. In the Tamengo Formation, the Cd isotope record points to overall low productivity levels. During intervals e1 and e2, $\delta^{114}Cd_{sw}$ values below BSE may indicate eutrophic conditions caused by high nutrient input during BIF weathering.
(vi) Similar to modern oceanographic dynamics, an intricate circulation-redox-productivity interplay controlled the extent of oxygenated shallow waters, which limited available benthic habitats for early animals in the late Ediacaran.

CRediT authorship contribution statement

Henrique Albuquerque Fernandes: Writing – original draft, Visualization, Investigation, Conceptualization. **Paulo César Boggiani:** Writing – review & editing, Supervision, Conceptualization. **Jesper Allan Frederiksen:** Writing – review & editing, Validation, Methodology. **Thales Pescarini:** Writing – review & editing, Conceptualization. **Vinicius Cardoso-Lucas:** Writing – review & editing, Visualization, Conceptualization. **Gustavo Paula-Santos:** Writing – review & editing, Validation, Conceptualization. **Eric Elias:** Writing – review & editing, Conceptualization. **Marly Babinski:** Writing – review & editing, Project administration, Funding acquisition, Conceptualization. **Juliana Leme:** . **Catherine V. Rose:** Writing – review & editing, Project administration, Conceptualization. **Ricardo Ivan Ferreira Trindade:** Writing – review & editing, Supervision, Project administration, Funding acquisition. **Robert Frei:** Validation, Supervision, Methodology, Funding acquisition, Conceptualization.

Declaration of competing interest

The authors declare that they have no known competing financial interests or personal relationships that could have appeared to influence the work reported in this paper.

Acknowledgements

We would like to acknowledge the São Paulo Research Foundation (FAPESP), through which we received funding under projects 2016/06114-6, 2020/16140-0, 2021/02628-3, 2023/02223-9, and 2024/08023-4. RIFT, MB, and PCB are fellows of the Brazilian National Council for Scientific and Technological Development (CNPq). We also acknowledge the Brazilian Federal Agency for Support and Evaluation of

Graduate Education (CAPES) for covering the APC. RF is grateful for the support and funding provided by the Independent Research Fund Denmark, grant 1026-00001B. We thank professors Claudio Gaucher, Fabricio Caxito, and Gabriel Jubé Uhlein for their thoughtful comments and suggestions that greatly improved the quality of this study. We also thank Toni Larsen and Cristina Nora Jensen de Olsen for laboratory assistance and the GRIND-ECT team for their support with the project. Finally, we thank two anonymous reviewers for their comments and suggestions.

Appendix A. Supplementary data

Supplementary data to this article can be found online at https://doi.org/10.1016/j.gr.2026.01.006.

References

Abouchami, W., Galer, S.J.G., de Baar, H.J.W., Alderkamp, A.C., Middag, R., Laan, P., Feldmann, H., Andreae, M.O., 2011. Modulation of the Southern Ocean cadmium isotope signature by ocean circulation and primary productivity. Earth Planet. Sci. Lett. 305, 83–91. https://doi.org/10.1016/j.epsl.2011.02.044.

Abouchami, W., Galer, S.J.G., de Baar, H.J.W., Middag, R., Vance, D., Zhao, Y., Klunder, M., Mezger, K., Feldmann, H., Andreae, M.O., 2014. Biogeochemical cycling of cadmium isotopes in the Southern Ocean along the Zero Meridian. Geochim. Cosmochim. Acta 127, 348–367. https://doi.org/10.1016/j.gca.2013.10.022.

Abouchami, W., Galer, S.J.G., Horner, T.J., Rehkämper, M., Wombacher, F., Xue, Z., Lambelet, M., Gault-Ringold, M., Stirling, C.H., Schönbächler, M., Shiel, A.E., Weis, D., Holdship, P.F., 2013. A common reference material for cadmium isotope studies - NIST SRM 3108. Geostand. Geoanal. Res. 37, 5–17. https://doi.org/10.1111/j.1751-908X.2012.00175.x.

Adorno, R.R., do Carmo, D.A., Germs, G., Walde, D.H.G., Denezine, M., Boggiani, P.C., Sousa e Silva, S.C., Vasconcelos, J.R., Tobias, T.C., Guimarães, E.M., Vieira, L.C., Figueiredo, M.F., Moraes, R., Caminha, S.A., Suarez, P.A.Z., Rodrigues, C.V., Caixeta, G.M., Pinho, D., Schneider, G., Muyamba, R., 2017. *Cloudina lucianoi* (Beurlen & Sommer, 1957), Tamengo formation, Ediacaran, Brazil: taxonomy, analysis of stratigraphic distribution and biostratigraphy. Precambr. Res. 301, 19–35. https://doi.org/10.1016/j.precamres.2017.08.023.

Afonso, J.W.L., Pereira, L.G., de Faria, B.A., Romero, G.R., Amorim, K.B., Basso, J.M.L., Trindade, R.I.F., 2024. Stratigraphical and sedimentological controls on the distribution of Cloudina bioclastic accumulations in the terminal Ediacaran Tamengo Formation (Corumbá Group), Brazil. Sediment. Geol. 463, 106580. https://doi.org/10.1016/j.sedgeo.2024.106580.

Alcott, L.J., Mills, B.J.W., Poulton, S.W., 2019. Stepwise Earth oxygenation is an inherent property of global biogeochemical cycling. Science 366 (6471), 1333–1337. https://doi.org/10.1126/science.aax6459.

Algeo, T.J., Lyons, T.W., 2006. Mo–total organic carbon covariation in modern anoxic marine environments: Implications for analysis of paleoredox and paleohydrographic conditions. Paleoceanography 21, 1. https://doi.org/10.1029/2004PA001112.

Almeida, F.F.M., 1965. Geologia da Serra da Bodoquena (Mato Grosso). DNPM 219, 1–96.

Alvarenga, C.J.S., Trompette, R., 1993. Evolução tectônica Brasiliana da Faixa Paraguai: a estruturação da região Cuiabá. Rev. Bras. Geocienc. 23 (1), 18–30.

Alvarenga, C.J.S., Boggiani, P.C., Babinski, M., Dardenne, M.A., Figueiredo, M., Santos, R.V., Dantas, E.L., 2009. Chapter 2 The Amazonian Palaeocontinent. Dev. Precambrian Geol. 16, 15–28. https://doi.org/10.1016/S0166-2635(09)01602-8.

Amorim, K.B., Afonso, J.W.L., Leme, J.de M., Diniz, C.Q.C., Rivera, L.C.M., Gómez-Gutiérrez, J.C., Boggiani, P.C., Trindade, R.I.F., 2020. Sedimentary facies, fossil distribution and depositional setting of the late Ediacaran Tamengo formation (Brazil). Sedimentology 67, 3422–3450. https://doi.org/10.1111/sed.12749.

Ansari, A.H., Pandey, S.K., Ahmad, S., Sharma, M., Govil, P., Chaddha, A.S., Sharma, A., 2023. High primary productivity in an Ediacaran shallow marine basin influenced by strong seasonal to perennial upwelling. Geol. Mag. 160 (8), 1607–1623. https://doi.org/10.1017/S0016756823000614.

Árting, T.B., Boggiani, P.C., Gaucher, C., Fernandes, H.A., Frei, R., 2023. Strong positive fractionation of chromium isotopes in iron formation of the Jacadigo Group (Brazil) - a link to enhanced atmospheric oxygenation during the late Neoproterozoic. Gondwana Res. 124, 39–60. https://doi.org/10.1016/j.gr.2023.06.017.

Asmerom, Y., Jacobsen, S.B., Knoll, A.H., Butterfield, N.J., Swett, K., 1991. Strontium isotopic variations of Neoproterozoic seawater: Implications for crustal evolution. Geochim. Cosmochim. Acta 55, 2883–2894. https://doi.org/10.1016/0016-7037(91)90453-C.

Babinski, M., Boggiani, P.C., Fanning, C.M., Fairchild, T.R., Simon, C.M., Sial, A.N., 2008. U-Pb shrimp geochronology and isotope chemostratigraphy (C, O, Sr) of the Tamengo Formation, southern Paraguay belt, Brazil. In: VI South American Symposium on Isotope Geology, Book of Abstracts, San Carlos de Bariloche, p. 160.

Babinski, M., McGee, B., Tokashiki, C.do C., Tassinari, C.C.G., Saes, G.S., Pinho, F.E.C., 2018. Comparing two arms of an orogenic belt during Gondwana amalgamation: age and provenance of the Cuiabá Group, northern Paraguay Belt, Brazil. J. S. Am. Earth Sci. 85, 6–42. https://doi.org/10.1016/j.jsames.2018.04.009.

Basu, A., Johnson, T.M., Sanford, R.A., 2014. Cr isotope fractionation factors for Cr(VI) reduction by a metabolically diverse group of bacteria. Geochim. Cosmochim. Acta 142, 349–361. https://doi.org/10.1016/j.gca.2014.07.024.

Bau, M., Koschinsky, A., 2009. Oxidative scavenging of cerium on hydrous Fe oxide: evidence from the distribution of rare earth elements and yttrium between Fe oxides and Mn oxides in hydrogenetic ferromanganese crusts. Geochem. J. 43 (1), 37–47. https://doi.org/10.2343/geochemj.1.0005.

Bauer, K.W., Gueguen, B., Cole, D.B., Francois, R., Kallmeyer, J., Planavsky, N., Crowe, S. A., 2018. Chromium isotope fractionation in ferruginous sediments. Geochim. Cosmochim. Acta 223, 198–215. https://doi.org/10.1016/j.gca.2017.10.034.

Becker-Kerber, B., Elmola, A.A., Zhuravlev, A., Gaucher, C., Simões, M.G., Prado, G.M.E. M., Vintaned, J.A.G., Fontaine, C., Lino, L.M., Sanchez, D.F., Galante, D., Paim, P.S. G., Callefo, F., Kerber, G., Meunier, A., El Albani, A., 2022. Clay templates in Ediacaran vendotaeniaceans: implications for the taphonomy of carbonaceous fossils. Geol. Soc. Am. Bull. 134, 1334–1346. https://doi.org/10.1130/B36033.1.

Berger, A., Frei, R., 2014. The fate of chromium during tropical weathering: a laterite profile from central madagascar. Geoderma 213, 521–532. https://doi.org/10.1016/j.geoderma.2013.09.004.

Berkner, L.V., Marshall, L.C., 1965. On the origin and rise of oxygen concentrations in the earth's atmosphere. J. Atmos. Sci. 22 (3), 225–261. https://doi.org/10.1175/1520-0469(1965)022<0225:OTOARO>2.0.CO;2.

Boggiani, P.C., 1998. Análise Estratigrafica da Bacia Corumbá (Neoproterozóico) - Mato Grosso do Sul. PhD Thesis, Universidade de São Paulo, São Paulo, 193p.

Boggiani, P.C., Fairchild, T.R., Coimbra, A.M., 1993. O Grupo Corumbá (Neoproterozoico-Cambriano) na região central da Serra da Bodoquena (Faixa Paraguai), Mato Grosso do Sul. ver. Bras. Geocienc. 23, 3, 301-305. Doi: 10.25249/0375-7536.1993233301305.

Boggiani, P.C., Gaucher, C., Sial, A.N., Babinski, M., Simon, C.M., Riccomini, C., Ferreira, V.P., Fairchild, T.R., 2010. Chemostratigraphy of the Tamengo Formation (Corumbá Group, Brazil): a contribution to the calibration of the Ediacaran carbon-isotope curve. Precambr. Res. 182 (4), 382–401. https://doi.org/10.1016/j.precamres.2010.06.003.

Bonnand, P., James, R.H., Parkinson, I.J., Connelly, D.P., Fairchild, I.J., 2013. The chromium isotopic composition of seawater and marine carbonates. Earth Planet. Sci. Lett. 382, 10–20.

Bowyer, F., Wood, R.A., Poulton, S.W., 2017. Controls on the evolution of Ediacaran metazoan ecosystems: a redox perspective. Geobiology 15 (4), 216–551. https://doi.org/10.1111/gbi.12232.

Bowyer, F.T., Wood, R.A., Yilales, M., 2024. Sea level controls on Ediacaran-Cambrian animal radiations. Sci. Adv. 10 (31), eado6462. https://doi.org/10.1126/sciadv.ado6462.

Boyle, E.A., Sclater, F., Edmond, J.M., 1976. On the marine geochemistry of cadmium. Nature 263, 42–44. https://doi.org/10.1038/263042a0.

Brandt, P., Hormann, V., Körtzinger, A., Visbeck, M., Krahmann, G., Stramma, L., Lumpkin, R., Schmid, C., 2010. Changes in the ventilation of the oxygen minimum zone of the tropical north Atlantic. J. Phys. Oceanogr. 40 (8), 1784–1801. https://doi.org/10.1175/2010JPO4301.1.

Bridgestock, L., Rehkämper, M., Flierdt, T.V., Murphy, K., Khondoker, R., Baker, A.R., Chance, R., Strekopytov, S., Humphreys-Williams, E., Achterberg, E.P., 2017. The Cd isotope composition of atmospheric aerosols from the Tropical Atlantic Ocean. Geophys. Res. Lett. 44 (6), 2932–2940. https://doi.org/10.1002/2017GL072748.

Bryan, A.L., Dickson, A.J., Dowdall, F., Homoky, W.B., Porcelli, D., Henderson, G.M., 2021. Controls on the cadmium isotope composition of modern marine sediments. Earth Planet. Sci. Lett. 565, 116946. https://doi.org/10.1016/j.epsl.2021.116946.

Bryne, R.H., Liu, X., Schijf, J., 1996. The influence of phosphate coprecipitation on rare earth distributions in natural waters. Geochim. Cosmochim. Acta 60 (17), 3341–3346. https://doi.org/10.1016/0016-7037(96)00197-4.

Campanha, G.A. da C., Boggiani, P.C., Sallun Filho, W., Sá, F.R. de, Zuquim, M. de P.S., Piacentini, T., 2011. A faixa de dobramento Paraguai na Serra da Bodoquena e depressão do Rio Miranda, Mato Grosso do Sul. Geol. USP, Sér. Cient. 11, 3, 79-96. Doi: 10.5327/z1519-874x2011000300005.

Canfield, D.E., Poulton, S.W., Knoll, A.H., Narbonne, G.M., Ross, G., Goldberg, T., Strauss, H., 2008. Ferruginous conditions dominated later neoproterozoic deep-water chemistry. Science 321 (5891), 949–952. https://doi.org/10.1126/science.1154499.

Canfield, D.E., Zhang, S., Frank, A.B., Wang, X., Wang, H., Su, J., Ye, Y., Frei, R., 2018. Highly fractionated chromium isotopes in Mesoproterozoic-aged shales and atmospheric oxygen. Nat. Commun. 9, 2871. https://doi.org/10.1038/s41467-018-05263-9.

Caxito, F.A., Frei, R., Uhlein, G.J., Dias, T.G., Árting, T.B., Uhlein, A., 2018. Multiproxy geochemical and isotope stratigraphy records of a neoproterozoic oxygenation event in the Ediacaran Sete Lagoas cap carbonate, Bambuí Group, Brazil. Chem. Geol. 481, 119–132. https://doi.org/10.1016/j.chemgeo.2018.02.007.

Caxito, F.A., Frei, R., Sial, A.N., Uhlein, G.J., Moura, W.A.L., Pereira, E., Rodrigues, R., 2023. Chromium isotopes track redox fluctuations in Proterozoic successions of the Chapada Diamantina, São Francisco craton, Brazil. Geology 51 (1), 69–74. https://doi.org/10.1130/G50344.1.

Caxito, F.A., Sperling, E., Fazio, G., Adorno, R.R., Denezine, M., Carmo, D.A.D., Giorgioni, M., Uhlein, G.J., Sial, A.N., 2024. A shift in redox conditions near the Ediacaran/Cambrian transition and its possible influence on early animal evolution, Corumbá Group, Brazil. Geosci. Front. 15 (4), 101810. https://doi.org/10.1016/j.gsf.2024.101810.

Chen, G., Bai, Y., Zeng, R.J., Qin, L., 2019a. Effects of different metabolic pathways and environmental parameters on Cr isotope fractionation during Cr(VI)reduction by extremely thermophilic bacteria. Geochim. Cosmochim. Acta 256, 135–146. https://doi.org/10.1016/j.gca.2019.01.002.

Chen, G., Han, J., Mu, Y., Yu, H., Qin, L., 2019b. Two-stage chromium isotope fractionation during microbial Cr(VI) reduction. Water Res. 148, 10–18. https://doi.org/10.1016/j.watres.2018.09.034.
Chen, X., Zhou, Y., Shields, G.A., 2022. Progress towards an improved Precambrian seawater $^{87}Sr/^{86}Sr$ curve. Earth-Sci. Rev. 224, 103869. https://doi.org/10.1016/j.earscirev.2021.103869.
Cole, D.B., Mills, D.B., Erwin, D.H., Sperling, E.A., Porter, S.M., Reinhard, C.T., Planavsky, N.J., 2020. On the co-evolution of surface oxygen levels and animals. Geobiology 18 (3), 260–281. https://doi.org/10.1111/gbi.12382.
Cordani, U.G., Fairchild, T.R., Ganade, C.E., Babinski, M., Leme, J.M., 2020. Dawn of metazoans: to what extent was this influenced by the onset of "modern-type plate tectonics"? Braz. J. Geol. 50 (2), e20190095. https://doi.org/10.1590/2317-4889202020190095.
Cui, H., Kaufman, A.J., Xiao, S., Peek, S., Cao, H., Min, X., Cai, Y., Siegel, Z., Liu, X.M., Peng, Y., Schiffbauer, J.D., Martin, A.J., 2016. Environmental context for the terminal Ediacaran biomineralization of animals. Geobiology 14, 344–363.
Daines, S.J., Mills, B.J.W., Lenton, T.M., 2017. Atmospheric oxygen regulation at low Proterozoic levels by incomplete oxidative weathering of sedimentary organic carbon. Nat. Commun. 8, 14379. https://doi.org/10.1038/ncomms14379.
D'Arcy, J., Gilleaudeau, G.J., Peralta, S., Gaucher, C., Frei, R., 2017. Redox fluctuations in the Early Ordovician oceans: an insight from chromium stable isotopes. Chem. Geol. 448, 1–12. https://doi.org/10.1016/j.chemgeo.2016.10.012.
De Baar, H.J.W., Bacon, M.P., Brewer, P.G., Bruland, K.W., 1985. Rare earth elements in the Pacific and Atlantic Oceans. Geochim. Cosmochim. Acta 49, 1943–1959. https://doi.org/10.1016/0016-7037(85)90089-4.
De Baar, H.J.W., Bruland, K.W., Schijf, J., van Heuven, S.M.A.C., Behrens, M.K., 2018. Low cerium among the dissolved rare earth elements in the central North Pacific Ocean. Geochim. Cosmochim. Acta 236, 5–40. https://doi.org/10.1016/j.gca.2018.03.003.
Diniz, C.Q.C., Leme, J. de M., Boggiani, P.C., 2021. New species of Macroalgae from Tamengo Formation, Ediacaran, Brazil. Front. Earth Sci. 9, 1–11. https://doi.org/10.3389/feart.2021.748876.
Dixon, J.L., 2008. Macro and micro nutrient limitation of microbial productivity in oligotrophic subtropical Atlantic waters. Environ. Chem. 5 (2), 135–142. https://doi.org/10.1071/EN07081.
Dohrmann, M., Wörheide, G., 2017. Dating early animal evolution using phylogenomic data. Sci. Rep. 7, 3599. https://doi.org/10.1038/s41598-017-03791-w.
dos Reis, M., Thawornwattana, Y., Angelis, K., Telford, M.J., Donoghue, P.C.J., Yang, Z., 2015. Uncertainty in the timing of origin of animals and the limits of precision in molecular timescales. Curr. Biol. 25, 2939–2950. https://doi.org/10.1016/j.cub.2015.09.066.
Døssing, L.N., Dideriksen, K., Stipp, S.L.S., Frei, R., 2011. Reduction of hexavalent chromium by ferrous iron: a process of chromium isotope fractionation and its relevance to natural environments. Chem. Geol. 285 (1–4), 157–166. https://doi.org/10.1016/j.chemgeo.2011.04.005.
Douville, E., Charlou, J.L., Oelkers, E.H., Bienvenu, P., Jove Colon, C.F., Donval, J.P., Fouquet, Y., Prieur, D., Appriou, P., 2002. The rainbow vent fluids (36°14′N, MAR): the influence of ultramafic rocks and phase separation on trace metal content in Mid-Atlantic Ridge hydrothermal fluids. Chem. Geol. 184, 37–48. https://doi.org/10.1016/S0009-2541(01)00351-5.
Downs, T.M., Schallenberg, M., Burns, C.W., 2008. Responses of lake phytoplankton to micronutrient enrichment: a study in two New Zealand lakes and an analysis of published data. Aquat. Sci. 70, 347–360. https://doi.org/10.1007/s00027-008-8065-6.
Droser, M.L., Tarhan, L.G., Gehling, J.G., 2017. The rise of animals in a changing environment: global ecological innovation in the late Ediacaran. Annu. Rev. Earth Planet. Sci. 45, 593–617. https://doi.org/10.1146/annurev-earth-063016-015645.
Druce, M., Stirling, C.H., Bostock, H.C., Rolison, J.M., 2022. Cadmium isotope systematics in sedimentary carbonate: extending the utility of the cadmium isotope palaeo-productivity proxy. Geochim. Cosmochim. Acta 339, 80–96. https://doi.org/10.1016/j.gca.2022.10.041.
Duda, J.P., Blumenberg, M., Thiel, V., Simon, K., Zhu, M., Reitner, J., 2014. Geobiology of a palaeoecosystem with Ediacara-type fossils: the Shibantan member (Dengying Formation, South China). Precambr. Res. 255, 48–62. https://doi.org/10.1016/j.precamres.2014.09.012.
Ellis, A.S., Johnson, T.M., Bullen, T.D., 2002. Chromium isotopes and the fate of hexavalent chromium in the environment. Science 295, 2060–2062. https://doi.org/10.1126/science.1068368.
Emerson, S.R., Huested, S.S., 1991. Ocean anoxia and the concentrations of molybdenum and vanadium in seawater. Mar. Chem. 34 (3–4), 177–196. https://doi.org/10.1016/0304-4203(91)90002-E.
Evans, S.D., Diamond, C.W., Droser, M.L., Lyons, T.W., 2018. Dynamic oxygen and coupled biological and ecological innovation during the second wave of the Ediacara Biota. Emerg. Top. Life Sci. 2 (2), 223–233. https://doi.org/10.1042/ETLS20170148.
Evans, S.D., Tu, C., Rizzo, A., Surprenant, R.L., Boan, P.C., McCandless, H., Marshall, N., Xiao, S., Droser, M.L., 2022. Environmental drivers of the first major animal extinction across the Ediacaran White Sea-Nama transition. PNAS 119 (46), e2207475119. https://doi.org/10.1073/pnas.2207475119.
Fairchild, T.R., Sanchez, E.A.M., Pacheco, M.L.A.F., Leme, J.M., 2012. Evolution of Precambrian life in the Brazilian geological record. J. Astrobiol. 11 (4), 309–323. https://doi.org/10.1017/S1473550412000183.
Farkaš, J., Frýda, J., Paulukat, C., Hathorne, E.C., Matoušková, Š., Rohovec, J., Frýdová, B., Francová, M., Frei, R., 2018. Chromium isotope fractionation between modern seawater and biogenic carbonates from the Great Barrier Reef, Australia: implications for the paleo-seawater $\delta^{53}Cr$ reconstruction. Earth Planet. Sci. Lett. 498, 140–151. https://doi.org/10.1016/j.epsl.2018.06.032.
Fazio, G., Guimarães, E.M., Walde, D.W.G., do Carmo, D.A., Adorno, R.R., Vieira, L.C., Denezine, M., da Silva, C.B., de Godoy, H.V., Borges, P.C., Pinho, D., 2019. Mineralogical and chemical composition of Ediacaran-Cambrian pelitic rocks of the Tamengo and Guaicurus formations, (Corumbá Group - MS, Brazil): stratigraphic positioning and paleoenvironmental interpretations. J. S. Am. Earth Sci. 90, 487–503. https://doi.org/10.1016/j.jsames.2018.11.025.
Fernandes, H.A., Boggiani, P.C., Afonso, J.W.L., Amorim, K.B., Trindade, R.I.F., 2022. Sedimentary and tectonic breccias at the base of the Ediacaran Tamengo formation (Corumbá Group): a comparative study. Braz. J. Geol. 52 (2), e20210062. https://doi.org/10.1590/2317-4889202220210062.
Fernandes, H.A., Boggiani, P.C., Frederiksen, J.A., Campos, M.D.R., Cardoso-Lucas, V., Freitas, B.T., Frei, R., 2025a. Rapid bioproductivity recovery following the Marinoan Glaciation: evidence from Sr-Cr-Cd isotopes and trace elements in the Morraria do Sul cap dolostone, Brazil. Chem. Geol. 673, 122548. https://doi.org/10.1016/j.chemgeo.2024.122548.
Fernandes, H.A., Paula-Santos, G.M., Pereira, L.G., Rimi, L.T., Pescarini, T., Elias, E., Bedoya-Rueda, C., Cardoso-Lucas, V., Rodrigues, L., Mazzamuto, K., Stama, L., Caetano-Filho, S., Babinski, M., Boggiani, P.C., et al., 2025b. Coevolution of life and environment during the Ediacaran-Cambrian transition: clues from litho-, bio-, and chemostratigraphy of the Corumbá Group, Brazil. Precambr. Res. 427, 107887. https://doi.org/10.1016/j.precamres.2025.107887.
Fernandes, H.A., Boggiani, P.C., Viana, A.Z., Caetano-Filho, S., Pereira, L.G., Freitas, B.T., Hippertt, J.P., Morais, L., Trindade, R.I.F., 2024. New advances on the carbon isotope and rare earth elements chemostratigraphy of the late Ediacaran Tamengo formation (Corumbá Group, Brazil). J. s. Am. Earth Sci. 133, 104696. https://doi.org/10.1016/j.jsames.2023.104696.
Frank, A.B., Klaebe, R.M., Frei, R., 2019. Fractionation Behavior of Chromium Isotopes during the Sorption of Cr (VI) on Kaolin and its Implications for using Black Shales as a Paleoredox Archive. Geochem. Geophys. Geosyst. 20, 2290–2302. https://doi.org/10.1029/2019gc008284.
Frederiksen, J.A., Klaebe, R.M., Farkaš, J., Swart, P.K., Frei, R., 2022a. Cadmium isotopes in Bahamas platform carbonates: a base for reconstruction of past surface water bioproductivity and their link with chromium isotopes. Sci. Total Environ. 806, 150565. https://doi.org/10.1016/j.scitotenv.2021.150565.
Frederiksen, J.A., Thibault, N., Gilleaudeau, J.G., Bjerrum, C.J., Moreau, J., Frei, R., 2024. Combined cadmium and chromium isotopes record a collapse of bioproductivity across the Cretaceous—Paleogene boundary in the Danish basin. Chem. Geol. 654, 122058. https://doi.org/10.1016/j.chemgeo.2024.122058.
Frederiksen, J.A., Wei, W., Rugen, E.J., Ling, H.F., Frei, R., 2022b. Cadmium isotopes in late Ediacaran–Early Cambrian Yangtze Platform carbonates – reconstruction of bioproductivity in ambient surface seawater. Palaeogeogr. Palaeoclimatol. Palaeoecol. 601, 111096. https://doi.org/10.1016/j.palaeo.2022.111096.
Frei, R., Gaucher, C., Boggiani, P.C., Frederiksen, J.A., Walker, S.R., Fernandes, H.A., Caxito, F., 2024. Surface water oxygenation and low bioproductivity during deposition of iron formation of the Jacadigo Group (Brazil): insights from combined cadmium – Chromium isotopes. Chem. Geol. 657, 122101. https://doi.org/10.1016/j.chemgeo.2024.122101.
Frei, R., Gaucher, C., Døssing, L.N., Sial, A.N., 2011. Chromium isotopes in carbonates — a tracer for climate change and for reconstructing the redox state of ancient seawater. Earth Planet. Sci. Lett. 312 (1–12), 114–125. https://doi.org/10.1016/j.epsl.2011.10.009.
Frei, R., Gaucher, C., Stolper, D., Canfield, D.E., 2013. Fluctuations in late Neoproterozoic atmospheric oxidation — Cr isotope chemostratigraphy and iron speciation of the late Ediacaran lower Arroyo del Soldado Group (Uruguay). Gondwana Res. 23 (2), 797–811. https://doi.org/10.1016/j.gr.2012.06.004.
Frei, R., Gaucher, C., Poulton, S.W., Canfield, D.E., 2009. Fluctuations in Precambrian atmospheric oxygenation recorded by chromium isotopes. Nature 461, 250–253. https://doi.org/10.1038/nature08266.
Frei, R., Døssing, L.N., Gaucher, C., Boggiani, P.C., Frei, K.M., Bech Árting, T., Crowe, S. A., Freitas, B.T., 2017. Extensive oxidative weathering in the aftermath of a late Neoproterozoic glaciation – evidence from trace element and chromium isotope records in the Urucum district (Jacadigo Group) and Puga iron formations (Mato Grosso do Sul, Brazil). Gondwana Res. 49, 1–20. https://doi.org/10.1016/j.gr.2017.05.003.
Frei, R., Poiré, D., Frei, K.M., 2014. Weathering on land and transport of chromium to the ocean in a subtropical region (Misiones, NW Argentina): a chromium stable isotope perspective. Chem. Geol. 381, 110–124. https://doi.org/10.1016/j.chemgeo.2014.05.015.
Freslon, N., Bayon, G., Toucanne, S., Bermell, S., Bollinger, C., Chéron, S., Etoubleau, J., Germain, Y., Khripounoff, A., Ponzevera, E., Rouget, M.-L., 2014. Rare earth elements and neodymium isotopes in sedimentary organic matter. Geochim. Cosmochim. Acta 140, 177–198. https://doi.org/10.1016/j.gca.2014.05.016.
Fuenzalida, R., Schneider, W., Garcés-Vargas, J., Bravo, L., Lange, C., 2009. Vertical and horizontal extension of the oxygen minimum zone in the eastern South Pacific Ocean. Deep Sea Res. Part II: Top. Stud. Oceanogr. 56 (16), 992–1003. https://doi.org/10.1016/j.dsr2.2008.11.001.
Gao, Y., Zhang, X., Xu, Y., Fang, C., Gong, Y., Shen, Y., 2020. High primary productivity during the Ediacaran period revealed by the covariation of paired C-isotopic records from South China. Precambr. Res. 349, 105411. https://doi.org/10.1016/j.precamres.2019.105411.
Gaucher, C., Boggiani, P.C., Sprechmann, P., Sial, A.N., Fairchild, T., 2003. Integrated correlation of the Vendian to Cambrian Arroyo del Soldado and Corumbá groups (Uruguay and Brazil): palaeogeographic, palaeoclimatic and palaeobiologic

implications. Precambr. Res. 120, 241–278. https://doi.org/10.1016/S0301-9268(02)00140-7.
Gaucher, C., Sprechmann, P., 2009. Chapter 9.1 Neoproterozoic Acritarch Evolution. In: Earth's Pre-Pleistocene Glacial Record. Dev. Precambrian Geol. 16, 247–260. Doi: 10.1016/S0166-2635(09)01622-3.
Gehling, J.G., Droser, M.L., 2013. How well do fossil assemblages of the Ediacara Biota tell time? Geology 41 (4), 447–450. https://doi.org/10.1130/G33881.1.
George, E., Stirling, C.H., Gault-Ringold, M., Ellwood, M.J., Middag, R., 2019. Marine biogeochemical cycling of cadmium and cadmium isotopes in the extreme nutrient-depleted subtropical gyre of the South West Pacific Ocean. Earth Planet. Sci. Lett. 514, 84–95. https://doi.org/10.1016/j.epsl.2019.02.031.
German, C.R., Elderfield, H., 1990. Application of the Ce anomaly as a paleoredox indicator: the ground rules. Paleoceanography 5, 823–833. https://doi.org/10.1029/PA005i005p00823.
German, C.R., Holliday, B.P., Elderfield, H., 1991. Redox cycling of rare earth elements in the suboxic zone of the Black Sea. Geochim. Cosmochim. Acta 55 (12), 3553–3558. https://doi.org/10.1016/0016-7037(91)90055-A.
Gilleaudeau, G.J., Frei, R., Kaufman, A.J., Kah, L.C., Azmy, K., Bartley, J.K., Chernyavskiy, P., Knoll, A.H., 2016. Oxygenation of the mid-Proterozoic atmosphere: clues from chromium isotopes in carbonates. Geochem. Perspect. Lett. 2, 178–187. https://doi.org/10.7185/geochemlet.1618.
Gong, Q., Li, F., Lu, C., Wang, H., Tang, H., 2021. Tracing seawater- and terrestrial-sourced REE signatures in detritally contaminated, diagenetically altered carbonate rocks. Chem. Geol. 570, 120169. https://doi.org/10.1016/j.chemgeo.2021.120169.
Grey, K., 2005. Ediacaran Palynology of Australia, 31. (Hornsby: Memoir, Association of Australasian Palaeontologists), 439.
Grey, K., Walter, M.R., Calver, C.R., 2003. Neoproterozoic biotic diversification: snowball Earth or aftermath of the Acraman impact? Geology 31 (5), 459–462. https://doi.org/10.1130/0091-7613(2003)031<0459:NBDSEO>2.0.CO;2.
Guinoiseau, D., Galer, S.J.G., Abouchami, W., Frank, M., Achterberg, E.P., Haug, G.H., 2019. Importance of cadmium sulfides for biogeochemical cycling of cd and its isotopes in oxygen deficient zones—a case study of the Angola Basin. Glob. Biogeochem. Cycles 33 (12), 1746–1763. https://doi.org/10.1029/2019GB006323.
Haley, B.A., Klinkhammer, G.P., McManus, J., 2004. Rare earth elements in pore waters of marine sediments. Geochim. Cosmochim. Acta 68 (6), 1265–1279. https://doi.org/10.1016/j.gca.2003.09.012.
Halverson, G.P., Dudás, F.Ö., Maloof, A.C., Bowring, S.A., 2007. Evolution of the $^{87}Sr/^{86}Sr$ composition of Neoproterozoic seawater. Palaeogeogr. Palaeoclimatol. Palaeocol. 256 (3–4), 103–129. https://doi.org/10.1016/j.palaeo.2007.02.028.
Halverson, G.P., Wade, B.P., Hurtgen, M.T., Barovich, K.M., 2010. Neoproterozoic chemostratigraphy. Precambr. Res. 182, 337–350. https://doi.org/10.1016/j.precamres.2010.04.007.
Hanson, C.E., Pattiaratchi, C.B., Waite, A.M., 2005. Sporadic upwelling on a downwelling coast: phytoplankton responses to spatially variable nutrient dynamics off the Gascoyne region of Western Australia. Cont. Shelf Res. 25 (12–13), 1561–1582. https://doi.org/10.1016/j.csr.2005.04.003.
He, X., Fang, Z., Gao, Y., Yu, X., Shen, Y., Qin, L., 2023. Redox heterogeneity of the Ediacaran ocean constrained by chromium isotopes. Geochim. Cosmochim. Acta 344, 178–189. https://doi.org/10.1016/j.gca.2022.12.024.
Hiatt, E.E., Pufahl, P.K., Guimarães da Silva, L., 2020. Iron and phosphorus biochemical systems and the Cryogenian-Ediacaran transition, Jacadigo basin, Brazil: implications for the Neoproterozoic oxygenation event. Precambr. Res. 337, 105533. https://doi.org/10.1016/j.precamres.2019.105533.
Hippertt, J.P.T.M., Rudnitzki, I.D., Morais, L., Freitas, B., Romero, G.R., Fernandes, H.A., Leite, M.G.P., Leme, J.M., Boggiani, P., Trindade, R.I.F., 2023. Sedimentary evolution and sequence stratigraphy of Ediacaran high-grade phosphorite–dolomite–shale successions of the Bocaina Formation (Corumbá Group), Central Brazil: implications for the Neoproterozoic phosphogenic event. Sedimentology 70 (7), 2371–2422. https://doi.org/10.1111/sed.13125.
Hippertt, T.M., Rudnitzki, I.D., Morais, L., Freitas, B.T., Nalini, H.A., Nogueira, L.B., Trindade, R.I.F., 2024. Assessing chemostratigraphic and biostratigraphic correlation of Ediacaran phosphorites (Bocaina, Khesen and Doushantuo Formations): diachronic, local signals of the Neoproterozoic phosphogenic-taphonomic even. Precambr. Res. 405, 107383. https://doi.org/10.1016/j.precamres.2024.107383.
Hohl, S.V., Becker, H., Jiang, S.Y., Ling, H.F., Guo, Q., Struck, U., 2017. Geochemistry of ediacaran cap dolostones across the yangtze platform, South China: implications for diagenetic modification and seawater chemistry in the aftermath of the marinoan glaciation. J. Geol. Soc. 174, 893–912. https://doi.org/10.1144/jgs2016-145.
Horner, T.J., Rickaby, R.E.M., Henderson, G.M., 2011. Isotopic fractionation of cadmium into calcite. Earth Planet. Sci. Lett. 312 (1–2), 243–253. https://doi.org/10.1016/j.epsl.2011.10.004.
Imai, N., Terashima, S., Itoh, S., Ando, A., 1996. 1996 compilation of analytical data on nine GSJ geochemical reference samples, "Sedimentary Rock Series". Geostand. Newsl. 20, 165–216. https://doi.org/10.1111/j.1751-908X.1996.tb00184.x.
Janssen, D.J., Abouchami, W., Galer, S.J.G., Purdon, K.B., Cullen, J.T., 2019. Particulate cadmium stable isotopes in the subarctic northeast Pacific reveal dynamic Cd cycling and a new isotopically light Cd sink. Earth Planet. Sci. Lett. 515, 67–78. https://doi.org/10.1016/j.epsl.2019.03.006.
Janssen, D.J., Rickli, J., Quay, P.D., White, A.E., Nasemann, P., Jaccard, S.L., 2020. Biological control of chromium redox and stable isotope composition in the surface ocean. Glob. Biogeochem. Cycles 34, 1, e2019GB006397. https://doi.org/10.1029/2019gb006397.
Janssen, D.J., Rickli, J., Wille, M., Steiner, O.S., Vogel, H., Dellwig, O., Berg, J.S., Bouffard, D., Lever, M.A., Hassler, C.S., Jaccard, S.L., 2022. Chromium cycling in redox-stratified basins challenges $\delta^{53}Cr$ paleoredox proxy applications. Geophys. Res. Lett. 49, 21, e2022GL099154. https://doi.org/10.1029/2022GL099154.
Joe-Wong, C., Weaver, K.L., Brown, S.T., Maher, K., 2021. Chromium isotope fractionation during reduction of Chromium(VI) by Iron(II/III)-bearing clay minerals. Geochim. Cosmochim. Acta 292, 235–253. https://doi.org/10.1016/j.gca.2020.09.034.
Kaufman, A.J., Jacobsen, S.B., Knoll, A.H., 1993. The Vendian record of Sr and C isotopic variations in seawater: implications for tectonics and paleoclimate. Earth Planet. Sci. Lett. 120 (3–4), 409–430. https://doi.org/10.1016/0012-821X(93)90254-7.
Kitchen, J.W., Johnson, T.M., Bullen, T.D., Zhu, J., Raddatz, A., 2012. Chromium isotope fractionation factors for reduction of Cr(VI) by aqueous Fe(II) and organic molecules. Geochim. Cosmochim. Acta 89, 190–201. https://doi.org/10.1016/j.gca.2012.04.049.
Klaebe, R., Swart, P., Frei, R., 2021. Chromium isotope heterogeneity on a modern carbonate platform. Chem. Geol. 573, 120227. https://doi.org/10.1016/j.chemgeo.2021.120227.
Knoll, A.H., 1992. The early evolution of eukaryotes: a geological perspective. Science 256 (5057), 622–627. https://doi.org/10.1126/science.1585174.
Knoll, A.H., Sperling, E.A., 2014. Oxygen and animals in Earth history. PNAS 111 (11), 3907–3908. https://doi.org/10.1073/pnas.1401745111.
Lacan, F., Francois, R., Ji, Y., Sherrell, R.M., 2006. Cadmium isotopic composition in the ocean. Geochim. Cosmochim. Acta 70, 5104–5118. https://doi.org/10.1016/j.gca.2006.07.036.
Lambelet, M., Rehkämper, M., Flierdt, T.V., Xue, Z., Kreissig, K., Coles, B., Porcelli, D., Andersson, P., 2013. Isotopic analysis of Cd in the mixing zone of Siberian rivers with the Arctic Ocean—new constraints on marine Cd cycling and the isotope composition of riverine Cd. Earth Planet. Sci. Lett. 361, 64–73. https://doi.org/10.1016/j.epsl.2012.11.034.
Lawrence, M.G., Greig, A., Collerson, K.D., Kamber, B.S., 2006. Rare earth element and yttrium variability in South East Queensland waterways. Aquat. Geochem. 12, 39–72. https://doi.org/10.1007/s10498-005-4471-8.
Leite, A.F.G.D., Fuck, R.A., Dantas, E.L., Ruiz, A.S., Moniê, P., Iemmolo, A., 2024. Tectonic significance of the late-Ediacaran syn-orogenic basin in the easternmost portion of the Paraguay Belt, Tocantins Province, central Brazil. J.S. Am. Earth Sci. 133, 104735. https://doi.org/10.1016/j.jsames.2023.104735.
Leme, J.M., Van Iten, H., Simões, M.G., 2022. A new conulariid (Cnidaria, Scyphozoa) from the terminal Ediacaran of Brazil. Front. Earth Sci. 10, 777746. https://doi.org/10.3389/feart.2022.777746.
Li, C., Love, G.D., Lyons, T.W., Fike, D.A., Sessions, A.L., Chu, X., 2010. A stratified redox model for the Ediacaran Ocean. Science 328 (5974), 80–83. https://doi.org/10.1126/science.1182369.
Ling, H.F., Chen, X., Li, D., Wang, D., Shields-Zhou, G.A., Zhu, M., 2013. Cerium anomaly variations in Ediacaran–earliest Cambrian carbonates from the Yangtze Gorges area, South China: implications for oxygenation of coeval shallow seawater. Precambr. Res. 225, 110–127. https://doi.org/10.1016/j.precamres.2011.10.011.
Liu, Y., Bowyer, F.T., Zhu, M., Xiong, Y., He, T., Han, M., Tang, X., Zhang, J., Poulton, S. W., 2024. Marine redox and nutrient dynamics linked to the Cambrian radiation of animals. Geology 52 (9), 729–734. https://doi.org/10.1130/G52220.1.
Marenco, P.J., Martin, K.R., Marenco, K.N., Barber, D.C., 2016. Increasing global ocean oxygenation and the Ordovician radiation: insights from Th/U of carbonates from the Ordovician of western Utah. Palaeogeogr. Palaeoclimatol. Palaeoecol. 458, 77–84. https://doi.org/10.1016/j.palaeo.2016.05.014.
McGee, B., Babinski, M., Trindade, R., Collins, A.S., 2018. Tracing final Gondwana assembly: age and provenance of key stratigraphic units in the southern Paraguay Belt, Brazil. Precambr. Res. 307, 1–33. https://doi.org/10.1016/j.precamres.2017.12.030.
McLennan, S., 1989. Chapter 7. Rare Earth elements In Sedimentary Rocks: Influence of Provenance and Sedimentary Processes. In: Lipin, B., McKay, G. (Eds.), Geochemistry and Mineralogy of Rare Earth Elements. De Gruyter, Berlin, Boston, pp. 169–200. https://doi.org/10.1515/9781501509032-010.
Meyer, M., Xiao, S., Gill, B.C., Schiffbauer, J.D., Chen, Z., Zhou, C., Yuan, X., 2014. Interactions between Ediacaran animals and microbial mats: Insights from Lamonte trevallis, a new trace fossil from the Dengying Formation of South China. Palaeogeogr. Palaeoclimatol. Palaeoecol. 396, 62–74. https://doi.org/10.1016/j.palaeo.2013.12.026.
Miletto, M., Wang, X., Planavsky, N.J., Luther, G.W., Lyons, T.W., Tebo, B.M., 2021. Marine microbial Mn(II) oxidation mediates Cr(III) oxidation and isotope fractionation. Geochim. Cosmochim. Acta 297, 101–119. https://doi.org/10.1016/j.gca.2021.01.008.
Mills, D.B., Ward, L.M., Jones, C., Sweeten, B., Forth, M., Treusch, A.H., Canfield, D.E., 2014. Oxygen requirements of the earliest animals. PNAS 111 (11), 4168–4172. https://doi.org/10.1073/pnas.1400547111.
Mills, D.B., Canfield, D.E., 2014. Oxygen and animal evolution: did a rise of atmospheric oxygen "trigger" the origin of animals? BioEssays 36 (12), 1145–1155. https://doi.org/10.1002/bies.201400101.
Morais, L., Fairchild, T.R., Freitas, B.T., Rudnitzki, I.D., Silva, E.P., Lahr, D., Moreira, A. C., Abrahão Filho, E.A., Leme, J.M., Trindade, R.I.F., 2021. Doushantuo-pertatataka—like acritarchs from the late ediacaran bocaina formation (Corumbá Group, Brazil). Front. Earth Sci. 9. https://doi.org/10.3389/feart.2021.787011.
Morais, L., Freitas, B.T., Fairchild, T.R., Clavijo-Arcos, R.E., Guillong, M., Vance, D., Campos, M.D.R., Babinski, M., Pereira, L.G., Leme, J.M., Boggiani, P.C., Osés, G., Rudnitzki, I.D., Galante, D., Rodrigues, F., Trindade, R.I.F., 2024. Dawn of diverse shelled and carbonaceous animal microfossils at ~571 Ma. Sci. Rep. 14, 14916. https://doi.org/10.1038/s41598-024-65671-4.
Nothdurft, L.D., Webb, G.E., Kamber, B.S., 2004. Rare earth element geochemistry of late Devonian reefal carbonates, Canning Basin, Western Australia: confirmation of a

seawater REE proxy in ancient limestones. Geochim. Cosmochim. Acta 68, 263–283. https://doi.org/10.1016/s0016-7037(03)00422-8.
Nozaki, Y., Zhang, J., Amakawa, H., 1997. The fractionation between Y and Ho in the marine environment. Earth Planet. Sci. Lett. 148, 329–340. https://doi.org/10.1016/S0012-821X(97)00034-4.
Nursall, J.R., 1959. Oxygen as a prerequisite to the origin of the Metazoa. Nature 183, 1170–1172. https://doi.org/10.1038/1831170b0.
Och, L.M., Shields-Zhou, G.A., 2012. The Neoproterozoic oxygenation event: environmental perturbations and biogeochemical cycling. Earth-Sci. Ver. 110, 26–57. https://doi.org/10.1016/j.earscirev.2011.09.004.
de Oliveira, R.S., Nogueira, A.C.R., Romero, G.R., Truckenbrodt, W., da Silva Bandeira, J. C., 2019. Ediacaran ramp depositional model of the Tamengo formation, Brazil. J. S. Am. Earth Sci. 96, 102348. https://doi.org/10.1016/j.jsames.2019.102348.
Osés, G.L., Wood, R., Romero, G.R., Prado, G.M.E.M., Bidola, P., Herzen, J., Pfeiffer, F., Stampar, S.N., Pacheco, M.L.A.F., 2022. Ediacaran Corumbella has a cataphract calcareous skeleton with controlled biomineralization. iScience 25 (12), 105676.
Ostrander, C.M., 2023. Mulling and nulling the coeval rise of Ediacaran oxygen and animals. Earth Planet. Sci. Lett. 614, 118187. https://doi.org/10.1016/j.epsl.2023.118187.
Ostrander, C.M., Owens, J.D., Nielsen, S.G., Lyons, T.W., Shu, Y., Chen, X., Sperling, E.A., Jiang, G., Johnston, D.T., Sahoo, S.K., Anbar, A.D., 2020. Thallium isotope ratios in shales from South China and northwestern Canada suggest widespread O_2 accumulation in marine bottom waters was an uncommon occurrence during the Ediacaran Period. Chem. Geol. 557, 119856. https://doi.org/10.1016/j.chemgeo.2020.119856.
Ostrander, C.M., Sahoo, S.K., Kendall, B., Jiang, G., Planavsky, N.J., Lyons, T.W., Nielsen, S.G., Owens, J.D., Gordon, G.W., Romaniello, S.J., Anbar, A.D., 2019. Multiple negative molybdenum isotope excursions in the Doushantuo formation (South China) fingerprint complex redox-related processes in the Ediacaran Nanhua Basin. Geochim. Cosmochim. Acta 261, 191–209. https://doi.org/10.1016/j.gca.2019.07.016.
Oze, C., Bird, D.K., Fendorf, S., 2007. Genesis of hexavalent chromium from natural sources in soil and groundwater. Proc. Natl. Acad. Sci. USA 104, 6544–6549. https://doi.org/10.1073/pnas.0701085104.
Pacheco, M.L.A.F., Galante, D., Rodrigues, F., Leme, J.M., Bidola, P., Hagardon, W., Stockmar, M., Herzen, J., Rudnitzki, I.D., Pfeiffer, F., Marques, A.C., 2018. Insights into the skeletonization, lifestyle, and affinity of the unusual Ediacaran Fossil Corumbella. PLoS One 10 (3), e0114219. https://doi.org/10.1371/journal.pone.0114219.
Parry, L.A., Boggiani, P.C., Condon, D.J., Garwood, R.J., Leme, J.D.M., McIlroy, D., Brasier, M.D., Trindade, R., Campanha, G.A.C., Pacheco, M.L.A.F., Diniz, C.Q.C., Liu, A.G., 2017. Ichnological evidence for meiofaunal bilaterians from the terminal Ediacaran and earliest Cambrian of Brazil. Nat. Ecol. Evol. 1, 1455–1464. https://doi.org/10.1038/s41559-017-0301-9.
Pattan, J.N., Pearce, N.J.G., Mislankar, P.G., 2005. Constraints in using Cerium-anomaly of bulk sediments as an indicator of paleo bottom water redox environment: a case study from the Central Indian Ocean Basin. Chem. Geol. 221 (3–4), 260–278. https://doi.org/10.1016/j.chemgeo.2005.06.009.
Paul, S.A.L., Haeckel, M., Bau, M., Bajracharya, R., Koschinsky, A., 2019. Small-scale heterogeneity of trace metals including rare earth elements and yttrium in deep-sea sediments and porewaters of the Peru Basin, southeastern equatorial Pacific. Biogeoschences 16 (24), 4829–4849. https://doi.org/10.5194/bg-16-4829-2019.
Paulukat, C., Døssing, L.N., Mondal, S.K., Voegelin, A.R., Frei, R., 2015. Oxidative release of chromium from Archean ultramafic rocks, its transport and environmental impact – a Cr isotope perspective on the Sukinda valley ore district (Orissa, India). Appl. Geochem. 59, 125–138. https://doi.org/10.1016/j.apgeochem.2015.04.016.
Paulukat, C., Gilleaudeau, G.J., Chernyavskiy, P., Frei, R., 2016. The Cr-isotope signature of surface seawater – a global perspective. Chem. Geol. 444, 101–109. https://doi.org/10.1016/j.chemgeo.2016.10.004.
Pereira, N.S., Voegelin, A.R., Paulukat, C., Sial, A.N., Ferreira, V.P., Frei, R., 2015. Chromium-isotope signatures in scleractinian corals from the Rocas Atoll, Tropical South Atlantic. Geobiology 14 (1), 54–67. https://doi.org/10.1111/gbi.12155.
Pickard, H., Palk, E., Schönbächler, M., Moore, R.E.T., Coles, B.J., Kreissig, K., Nilsson-Kerr, K., Hammond, S.J., Takazawa, E., Hémond, C., Tropper, P., Barfod, D.N., Rehkämper, M., 2022. The cadmium and zinc isotope compositions of the silicate Earth – implications for terrestrial volatile accretion. Geochim. Cosmochim. Acta 338, 165–180. https://doi.org/10.1016/j.gca.2022.09.041.
Price, N.M., Morel, F.M.M., 1990. Cadmium and cobalt substitution for zinc in a marine diatom. Nature 344, 658–660. https://doi.org/10.1038/344658a0.
Ramos, M.E.A.F., Giorgioni, M., Walde, D.H.G., Carmo, D.A., Fazio, G., Vieira, L.C., Denezine, M., Santos, R.V., Adôrno, R.R., Guida, L.L., 2022. New facies model and carbon isotope stratigraphy for an ediacaran carbonate platform from South America (Tamengo formation) — Corumbá Group, SW Brazil. Front. Earth Sci. 10, 1–24. https://doi.org/10.3389/feart.2022.749066.
Reinhard, C.T., Planavsky, N.J., Robbins, L.J., Partin, C.A., Gill, B.C., Lalonde, S.V., Bekker, A., Konhauser, K.O., Lyons, T.W., 2013. Proterozoic ocean redox and biogeochemical stasis. PNAS 110 (14), 5357–5362. https://doi.org/10.1073/pnas.1208622110.
Reinhard, C.T., Planavsky, N.J., Wang, X., Fischer, W.W., Johnson, T.M., Lyons, T.W., 2014. The isotopic composition of authigenic chromium in anoxic marine sediments: a case study from the Cariaco Basin. Earth Planet. Sci. Lett. 407, 9–18. https://doi.org/10.1016/j.epsl.2014.09.024.
Richards, F.A., 1958. Chapter 9: Oxygen in the Ocean. Treatise on Marine Ecology and Paleoecology. Doi: 10.1130/MEM67V1-p185.
Richter, F.M., Rowley, D.B., DePaolo, D.J., 1992. Sr isotope evolution of seawater: the role of tectonics. Earth Planet. Sci. Lett. 109, 11–23. https://doi.org/10.1016/0012-821X(92)90070-C.
Ripperger, S., Rehkämper, M., Porcelli, D., Halliday, A.N., 2007. Cadmium isotope fractionation in seawater - a signature of biological activity. Earth Planet. Sci. Lett. 261, 670–684. https://doi.org/10.1016/j.epsl.2007.07.034.
Rodler, A., Sánchez-Pastor, N., Fernández-Díaz, L., Frei, R., 2015. Fractionation behavior of chromium isotopes during coprecipitation with calcium carbonate: implications for their use as paleoclimatic proxy. Goechim. Cosmochim. Acta 164, 221–235. https://doi.org/10.1016/j.gca.2015.05.021.
Rodler, A.S., Frei, R., Gaucher, C., Germs, G.J.B., 2016. Chromium isotope, REE and redox-sensitive trace element chemostratigraphy across the late Neoproterozoic Ghaub glaciation, Otavi Group, Namibia. Precambr. Res. 286, 234–249. https://doi.org/10.1016/j.precamres.2016.10.007.
Rose, C.V., Prave, A.R., Bergmann, K.D., Condon, D.J., Kasemann, S.A., Macdonald, F.A., Hoffmann, K.-H., Trindade, R.I.F., Zhu, M., 2019. Project report: grinding through the Ediacaran-Cambrian transition. Commun. Geol. Surv. Namib. 21.
Rugen, E.J., Ineson, J.R., Frei, R., 2022. Low oxygen seawater and major shifts in the paleoenvironment towards the terminal Ediacaran: insights from the Portfjeld formation, North Greenland. Precambr. Res. 379, 106781. https://doi.org/10.1016/j.precamres.2022.106781.
Rühlemann, C., Müller, P.J., Schneider, R.R., 1999. Organic Carbon and Carbonate as Paleoproductivity Proxies: Examples from High and Low Productivity Areas of the Tropical Atlantic. In: Use of Proxies in Paleoceanography 315-344.
Schauble, E., Rossman, G.R., Taylor Jr., H.P., 2004. Theoretical estimates of equilibrium chromium-isotope fractionation. Chem. Geol. 205 (1–2), 99–114. https://doi.org/10.1016/j.chemgeo.2003.12.015.
Scheiderich, K., Amini, M., Holmden, C., Francois, R., 2015. Global variability of chromium isotopes in seawater demonstrated by Pacific, Atlantic, and Arctic Ocean samples. Earth Planet. Sci. Lett. 423, 87–97. https://doi.org/10.1016/j.epsl.2015.04.030.
Schmitt, A.D., Galer, S.J.G., Abouchami, W., 2009. Mass-dependent cadmium isotopic variations in nature with emphasis on the marine environment. Earth Planet. Sci. Lett. 277, 262–272. https://doi.org/10.1016/j.epsl.2008.10.025.
Schoenberg, R., Zink, S., Staubwasser, M., von Blanckenburg, F., 2008. The stable Cr isotope inventory of solid Earth reservoirs determined by double spike MC-ICP-MS. Chem. Geol. 249 (3–4), 294–306. https://doi.org/10.1016/j.chemgeo.2008.01.009.
Scholz, F., 2018. Identifying oxygen minimum zone-type biogeochemical cycling in Earth history using inorganic geochemical proxies. Earth-Sci. Rev. 184, 29–45. https://doi.org/10.1016/j.earscirev.2018.08.002.
Shields, G.A., 2007. A normalised seawater strontium isotope curve: possible implications for Neoproterozoic-Cambrian weathering rates and the further oxygenation of the earth. eEarth 2, 35–42. https://doi.org/10.5194/ee-2-35-2007.
Shields, G., Stille, P., 2001. Diagenetic constraints on the use of cerium anomalies as palaeoseawater redox proxies: an isotopic and REE study of Cambrian phosphorites. Chem. Geol. 175 (1–2), 29–48. https://doi.org/10.1016/S0009-2541(00)00362-4.
Sholkovitz, E.R., Landing, W.M., Lewis, B.L., 1994. Ocean particle chemistry: the fractionation of rare earth elements between suspended particles and seawater. Geochim. Cosmochim. Acta 58, 1567–1579. https://doi.org/10.1016/0016-7037(94)90559-2.
Sieber, M., Conway, T.M., de Souza, G.F., Obata, H., Takano, S., Sohrin, Y., Vance, D., 2019. Physical and biogeochemical controls on the distribution of dissolved cadmium and its isotopes in the Southwest Pacific Ocean. Chem. Geol. 511, 494–509. https://doi.org/10.1016/j.chemgeo.2018.07.021.
Sieber, M., Lanning, N.T., Bunnell, Z.B., Bian, X., Yang, S.C., Marsay, C.M., Landing, W. M., Buck, C.S., Fitzsimmons, J.N., John, S.G., Conway, T.M., 2023. Biological, Physical, and Atmospheric Controls on the distribution of Cadmium and its Isotopes in the Pacific Ocean. Glob. Biogeochem. Cycles 37, 2, e2022GB007441. https://doi.org/10.1029/2022GB007441.
Sikora, E.R., Johnson, T.M., Bullen, T.D., 2008. Microbial mass-dependent fractionation of chromium isotopes. Geochim. Cosmochim. Acta 72, (15), 3631–3641. https://doi.org/10.1016/j.gca.2008.05.051.
Spangenberg, J.E., Bagnoud-Velásquez, M., Boggiani, P.C., Gaucher, C., 2014. Redox variations and bioproductivity in the Ediacaran: evidence from inorganic and organic geochemistry of the Corumbá Group, Brazil. Gondwana Res. 26 (3–4), 1186–1207. https://doi.org/10.1016/j.gr.2013.08.014.
Sperling, E.A., Stockey, R.G., 2018. The temporal and environmental context of early animal evolution: considering all the ingredients of an "explosion". Integr. Comp. Biol. 58 (4), 605–622. https://doi.org/10.1093/icb/icy088.
Stoll, J.T., Larson, J.H., Bailey, S.W., Blackwood, C.B., Costello, D.M., 2024. Macro- and micronutrient effects on phytoplankton in Green Bay, Lake Michigan, and the western basin of Lake Erie. J. Phycol. 60 (6), 1514–1527. https://doi.org/10.1111/jpy.13519.
Swart, P.K., 2015. The geochemistry of carbonate diagenesis: the past, present and future. Sedimentology 62, 1233–1304. https://doi.org/10.1111/sed.12205.
Tang, J., Johannesson, K.H., 2010. Ligand extraction of rare earth elements from aquifer sediments: implications for rare earth element complexation with organic matter in natural waters. Geochim. Cosmochim. Acta 74 (23), 6690–6705. https://doi.org/10.1016/j.gca.2010.08.028.
Tarhan, L.G., Droser, M.L., Cole, D.B., Gehling, J.G., 2018. Ecological expansion and extinction in the late Ediacaran: weighing the evidence for environmental and biotic drivers. Integr. Comp. Biol. 58 (4), 688–702. https://doi.org/10.1093/icb/icy020.
Thamdrup, B., Dalsgaard, T., Revsbech, N.P., 2012. Widespread functional anoxia in the oxygen minimum zone of the Eastern South Pacific. Deep Sea Res. Part I: Oceanogr. Res. Pap. 65, 36–45. https://doi.org/10.1016/j.dsr.2012.03.001.

Thiede, J., Jünger, B., 1992. Faunal and floral indicators of ocean coastal upwelling (NW African and Peruvian Continental Margins). Geol. Soc. Lond. Spec. Publ. 64, 47–76. https://doi.org/10.1144/GSL.SP.1992.064.01.04.

Tostevin, R., Shields, G.A., Tarbuck, G.M., He, T., Clarkson, M.O., Wood, R.A., 2016a. Effective use of cerium anomalies as a redox proxy in carbonate-dominated marine settings. Chem. Geol. 438, 146–162. https://doi.org/10.1016/j.chemgeo.2016.06.027.

Tostevin, R., Wood, R.A., Shields, G.A., Poulton, S.W., Guilbaud, R., Bowyer, F., Penny, A.M., He, T., Curtis, A., Hoffmann, K.H., Clarkson, M.O., 2016b. Low-oxygen waters limited habitable space for early animals. Nat. Commun. 7, 12818. https://doi.org/10.1038/ncomms12818.

Tribovillard, N., Algeo, T.J., Lyons, T., Riboulleau, A., 2006. Trace metals as paleoredox and paleoproductivity proxies: an update. Chem. Geol. 232 (1–2), 12–32. https://doi.org/10.1016/j.chemgeo.2006.02.012.

Trompette, R., De Alvarenga, C.J.S., Walde, D., 1998. Geological evolution of the Neoproterozoic Corumba graben system (Brazil). Depositional context of the stratified Fe and Mn ores of the Jacadigo Group. J. S. Am. Earth Sci. 11, 6, 587–597. https://doi.org/10.1016/S0895-9811(98)00036-4.

Walde, D.H.G., Do Carmo, D.A., Guimarães, E.M., Vieira, L.C., Erdtmann, B.D., Sanchez, E.A.M., Adorno, R.R., Tobias, T.C., 2015. New aspects of Neoproterozoic-Cambrian transition in the Corumbá region (state of Mato Grosso do Sul, Brazil). Ann. Paleontol. 101, 213–224. https://doi.org/10.1016/j.annpal.2015.07.002.

Wang, W., Lough, A.J.M., Goring-Harford, H., Flanagan, O., González-Santana, D., Resing, J., Connelly, D., Lohan, M.C., Tagliabue, A., James, R.H., 2023. Fractionation of iron and chromium isotopes in hydrothermal plumes from the northern Mid-Atlantic Ridge. Earth Planet. Sci. Lett. 624, 118468. https://doi.org/10.1016/j.epsl.2023.118468.

Wei, W., Frei, R., Chen, T.Y., Klaebe, R., Liu, H., Li, D., Wei, H.Y., Ling, H.F., 2018. Marine ferromanganese oxide: a potentially important sink of light chromium isotopes? Chem. Geol. 495, 90–103. https://doi.org/10.1016/j.chemgeo.2018.08.006.

Wei, W., Frei, R., Gilleaudeau, G.J., Li, D., Wei, G.Y., Huang, F., Ling, H.F., 2020. Variations of redox conditions in the atmosphere and Yangtze Platform during the Ediacaran-Cambrian transition: Constraints from Cr isotopes and Ce anomalies. Palaeogeogr. Palaeoclimat. Palaeoecol. 543, 109598. https://doi.org/10.1016/j.palaeo.2020.109598.

Williams, J.J., Mills, B.J.W., Lenton, T.M., 2019. A tectonically driven Ediacaran oxygenation event. Nat. Commun. 10, 2690. https://doi.org/10.1038/s41467-019-10286-x.

Wood, R.A., Erwin, D.H., 2017. Innovation not recovery: dynamic redox promotes metazoan radiations. Biol. Rev. 93 (2), 863–873. https://doi.org/10.1111/brv.12375.

Wood, R.A., Poulton, S.W., Prave, A.R., Hoffmann, K.H., Clarkson, M.O., Guilbaud, R., Lyne, J.W., Tostevin, R., Bowyer, F., Penny, A.M., Curtis, A., Kasemann, S.A., 2015. Dynamic redox conditions control late Ediacaran metazoan ecosystems in the Nama Group, Namibia. Precambr. Res. 261, 252–271. https://doi.org/10.1016/j.precamres.2015.02.004.

Xu, D., Wang, X., Zhu, J.M., Jiang, G., Shi, X., Wang, X., Sahoo, S.K., 2022. Chromium isotope evidence for oxygenation events in the Ediacaran ocean. Geochim. Cosmochim. 323, 258–275. https://doi.org/10.1016/j.gca.2022.02.019.

Yamamoto, A., Abe-Ouchi, A., Shigemitsu, M., Oka, A., Takahashi, K., Ohgaito, R., Yamanaka, Y., 2015. Global deep ocean oxygenation by enhanced ventilation in the Southern Ocean under long-term global warming. Glob. Biogeochem. Cycles 29 (10), 1801–1815. https://doi.org/10.1002/2015GB005181.

Zhang, Q., Amor, K., Galer, S.J.G., Thompson, I., Porcelli, D., 2019. Using stable isotope fractionation factors to identify Cr(VI) reduction pathways: metal-mineral-microbe interactions. Water Res. 151, 98–109. https://doi.org/10.1016/j.watres.2018.11.088.

Zhang, J., Nozaki, Y., 1996. Rare earth elements and yttrium in seawater: ICP-MS determinations in the East Caroline, Coral Sea, and South Fiji basins of the western South Pacific Ocean. Geochim. Cosmochim. Acta 60, 4631–4644. https://doi.org/10.1016/S0016-7037(96)00276-1.

Zhang, K., Shields, G.A., 2023. Early diagenetic mobilization of rare earth elements and implications for the Ce anomaly as a redox proxy. Chem. Geol. 635, 121619. https://doi.org/10.1016/j.chemgeo.2023.121619.

Zhang, S., Wang, X., Wang, H., Bjerrum, C.J., Hammarlund, E.U., Costa, M.M., Connelly, J.N., Zhang, B., Su, J., Canfield, D.E., 2016. Sufficient oxygen for animal respiration 1,400 million years ago. PNAS 113 (7), 1731–1736. https://doi.org/10.1073/pnas.1523449113.

Zhang, S., Wang, H., Wang, X., Ye, Y., 2021. The mesoproterozoic oxygenation event. Sci. China Earth Sci. 64, 2043–2068. https://doi.org/10.1007/s11430-020-9825-x.

Zhou, Y., von Strandmann, P.A.E.P., Zhu, M., Ling, H., Manning, C., Li, D., He, T., Shields, G.A., 2020. Reconstructing tonian seawater 87Sr/86Sr using calcite microspar. Geology 48, 462–467. https://doi.org/10.1130/G46756.1.